cmgh
CELLULAR AND MOLECULAR GASTROENTEROLOGY AND HEPATOLOGY

ORIGINAL RESEARCH

Pigment Epithelium-Derived Factor (PEDF) Inhibits Wnt/β-catenin Signaling in the Liver

Petr Protiva,[1,2,*] Jingjing Gong,[1,*] Bharath Sreekumar,[2] Richard Torres,[3] Xuchen Zhang,[2] Glenn S. Belinsky,[1] Mona Cornwell,[4] Susan E. Crawford,[4] Yasuko Iwakiri,[1] and Chuhan Chung[1,2]

[1]Department of Medicine, Yale University School of Medicine, New Haven, Connecticut; [2]VA CT Healthcare System, West Haven, Connecticut; [3]Department of Laboratory Medicine, Yale University School of Medicine, New Haven, Connecticut; [4]Department of Pathology, St. Louis University School of Medicine, St. Louis, Missouri

SUMMARY

The absence of pigment epithelium-derived factor (PEDF) in hepatocellular carcinoma (HCC) enhances Wnt/β-catenin signaling. Genomic profiling of PEDF knockout livers correlates with gene expression signatures of human HCC associated with aberrant Wnt/β-catenin signaling. PEDF is an endogenous inhibitor of Wnt/β-catenin signaling.

BACKGROUND & AIMS: Pigment epithelium-derived factor (PEDF) is a secretory protein that inhibits multiple tumor types. PEDF inhibits the Wnt coreceptor, low-density lipoprotein receptor-related protein 6 (LRP6), in the eye, but whether the tumor-suppressive properties of PEDF occur in organs such as the liver is unknown.

METHODS: Wnt-dependent regulation of PEDF was assessed in the absence and presence of the Wnt coreceptor LRP6. Whole genome expression analysis was performed on PEDF knockout (KO) and control livers (7 months). Interrogation of Wnt/β-catenin signaling was performed in whole livers and human hepatocellular carcinoma (HCC) cell lines after RNA interference of PEDF and restoration of a PEDF-derived peptide. Western diet feeding for 6 to 8 months was used to evaluate whether the absence of PEDF was permissive for HCC formation (n = 12/group).

RESULTS: PEDF levels increased in response to canonical Wnt3a in an LRP6-dependent manner but were suppressed by noncanonical Wnt5a protein in an LRP6-independent manner. Gene set enrichment analysis (GSEA) of PEDF KO livers revealed induction of pathways associated with experimental and human HCC and a transcriptional profile characterized by Wnt/β-catenin activation. Enhanced Wnt/β-catenin signaling occurred in KO livers, and PEDF delivery in vivo reduced LRP6 activation. In human HCC cells, RNA interference of PEDF led to increased levels of activated LRP6 and β-catenin, and a PEDF 34-mer peptide decreased LRP6 activation and β-catenin signaling, and reduced Wnt target genes. PEDF KO mice fed a Western diet developed sporadic well-differentiated HCC. Human HCC specimens demonstrated decreased PEDF staining compared with hepatocytes.

CONCLUSIONS: PEDF is an endogenous inhibitor of Wnt/β-catenin signaling in the liver. *(Cell Mol Gastroenterol Hepatol 2015;1:535–549; http://dx.doi.org/10.1016/j.jcmgh.2015.06.006)*

Keywords: Extracellular Matrix; PEDF; Wnt/β-Catenin.

Hepatocellular carcinoma (HCC) is a major cause of cancer-related deaths worldwide.[1] Genomic profiling has classified HCC based on molecular "signatures" that correlate with biological characteristics and clinical outcomes.[2,3] One finding from these studies is the role of the extracellular matrix (ECM) in determining tumor behavior.[4–6] For instance, modulators of the ECM can activate developmental pathways such as Wnt/β-catenin signaling, thereby connecting liver fibrosis to a signaling pathway that drives hepatocarcinogenesis.[3]

Pigment epithelium-derived factor (PEDF) is a circulating 50-kDa protein with ECM binding domains and broad tumor suppressive properties.[7–10] In PEDF knockout (KO) mice, stromal abnormalities occur in multiple organs including the prostate, pancreas, and liver.[11–15] Endogenous liver levels of PEDF decline in experimental and human cirrhosis, and PEDF delivery ameliorates experimental liver fibrosis.[14,16] PEDF null mice crossed with the $Kras^{G12D}$ mice resulted in marked stromal changes in the pancreas and an invasive malignant phenotype not seen in the $Kras^{G12D}$ mutant mice alone.[15] These results indicate that PEDF regulates tissue matrix quiescence and its absence is permissive for malignant transformation.

The antitumor properties of PEDF are typically attributed to an antiangiogenic effect.[10,17] PEDF, however, inhibits tumor cells in culture, indicating other mechanisms.[17,18] Park et al[19] identified PEDF's ability to inhibit

*P.P. and J.G. contributed equally to this work.

Abbreviations used in this paper: **BABB, benzyl alcohol/benzyl benzoate; CM, conditioned medium; ECM, extracellular matrix; ERK, extracellular signal-regulated kinase; FDR, false-discovery rate; GAPDH, glyceraldehyde-3-phosphate dehydrogenase; GO, Gene Ontology; GSEA, gene set enrichment analysis; GSK, glycogen synthase kinase; HCC, hepatocellular carcinoma; KO, knockout; LRP6, low-density lipoprotein receptor-related protein 6; PCR, polymerase chain reaction; PEDF, pigment epithelium-derived factor; SHG, second harmonic generation; siRNA, small interfering RNA; WT, wild type.**

Most current article

2352-345X
http://dx.doi.org/10.1016/j.jcmgh.2015.06.006

Wnt/β-catenin signaling in the eye with avid binding to the Wnt coreceptor, low-density lipoprotein receptor-related protein 6 (LRP6). Whether PEDF has systemic effects beyond the eye and inhibits tumor development through an inhibitory effect on Wnt/β-catenin signaling is unclear. Because PEDF is most highly expressed by the liver, a finding recently confirmed in the Human Protein Atlas,[20,21] and modulates Wnt/β-catenin signaling,[19,22] we asked whether PEDF functions as an LRP6 antagonist in the liver.

We establish that canonical Wnt3a ligand directly regulates PEDF levels. PEDF, in turn, inhibits Wnt/β-catenin signaling. Consistent with this, livers from PEDF KO mice have a transcriptional profile closely aligned with murine models of hepatocarcinogenesis and human HCC characterized by aberrant Wnt/β-catenin signaling. Knockout and knock-in experiments demonstrate that PEDF inhibits Wnt/β-catenin signaling in murine livers and human HCC cells through its ability to inhibit LRP6 and β-catenin activity. Finally, a chronic Western diet elicited sporadic HCC formation in PEDF KO mice, while the human HCC specimens demonstrated diminished PEDF staining.

Materials and Methods

Human Hepatocellular Carcinoma, Animals, and Liver Tumor Induction

Archival human HCC tissues and their corresponding adjacent livers from 14 patients were obtained from the VA Connecticut Healthcare System according to an approved institutional review board protocol. The PEDF KO mice were bred with age-matched wild-type (WT) littermates on the C57BL/6J background to generate heterozygous breeding pairs, and then PEDF KO and WT offspring were backcrossed for more than 10 generations.[11] The mice were genotyped using a commercially available polymerase chain reaction (PCR) kit (Sigma-Aldrich, St. Louis, MO). All procedures were approved by the Institutional Animal Care and Use Committee of VA CT Healthcare System. A commercial Western diet—TestDiet 4342 (TestDiet, St. Louis, MO): energy (% kcal) from fat (40%), carbohydrate (44%), protein (16%)—or standard chow was given for 26 to 32 weeks to PEDF KO and age-matched controls (n = 12/group) starting at 8 to 12 weeks of age.

RNA Extraction and Gene Arrays

Frozen whole liver tissue from five PEDF KO animals and WT controls were maintained in liquid nitrogen until total RNA extraction using the TRIzol method (Invitrogen, Carlsbad, CA). TRIzol-extracted RNA was further purified using the Qiagen RNeasy kit (Qiagen, Valencia, CA), yielding high-quality RNA suitable for microarray analyses (RNA integrity number >9). The RNA quality was verified using Agilent 2100 Bioanalyzer (Agilent Technologies, Palo Alto, CA), and the RNA was quantified by NanoDrop (NanoDrop Technologies, Wilmington, DE). For gene expression analysis, 500 ng of total RNA was used to generate biotin-labeled cRNA using the Illumina Total RNA amplification and labeling kit (Ambion, Austin, TX) according to the manufacturer's instructions. The biotinylated cRNA was labeled with fluorescent dye at the Yale Keck Genomic Core Facility (West Haven, CT), hybridized onto a MouseRef-8 v2.0 Expression BeadChip expression array bead chip (Illumina, San Diego, CA) and scanned.

Expression data were analyzed by Genespring GX12 software (Agilent Technologies) after normalization by 75th percentile shift. Only genes with a present signal (signal above background noise) in more than 50% of samples were included in the analysis. Group samples with gene expression correlation coefficients $\leq$0.95 were excluded (one KO sample). For the statistical analysis, replicate samples were averaged. Differences in gene expression were determined using a moderated t test, and multiple hypothesis testing adjustment was made using Benjamini–Hochberg method at a false-discovery rate (FDR) $\leq$ .05 and by adding a fold expression cutoff of 1.3. Genes differentially expressed in KO mice versus WT were subjected to Gene Ontology (GO) (http://www.geneontology.org) and WikiPathways (http://www.wikipathways.org) enrichment analysis using the hypergeometric test corrected by Benjamini–Yekutieli method at FDR $q \leq$0.05.

To further extend the analysis, gene set enrichment analysis (GSEA) was used (http://www.broadinstitute.org/gsea). GSEA is a computational method that determines whether an a priori defined set of genes shows statistically significant differences between two phenotypes.[23] To identify the gene sets that were statistically significantly enriched, we created a rank-order list by gene expression differences between KO and WT sets. Gene Ontology, KEGG pathways (http://www.genome.jp), Reactome (http://www.reactome.org), Biocarta (http://www.biocarta.org), Pathway interaction database (http://pid.nci.nih.gov), and curated gene sets reflecting changes induced by various chemical and genetic perturbances were used to interpret results. FDR q value was used to rank the results. Gene sets enriched at FDR q value $\leq$ .05 and nominal $P <$ .05 were considered statistically significant. Gene array data were deposited at http://www.ncbi.nlm.nih.gov/geo/query/acc.cgi?acc=GSE63643.

PEDF and PEDF Peptide Restoration

Human full-length PEDF was generated in human embryonic kidney cells as described elsewhere, and its purity confirmed using Coomassie and silver staining (Invitrogen).[12] PEDF was administered (25 μg/kg bwt) by intraperitoneal injection on alternate days for a period of 4 weeks.[24] A 34-mer of human PEDF corresponding to amino acids 44–77 has been previously shown to inhibit neovascularization and inhibit tumor growth, but its role in Wnt signaling is unclear.[17,25] We interrogated Wnt signaling with a 34-mer that was commercially obtained (NeoBiolab, Cambridge, MA) and used at a concentration of 100μM to evaluate Wnt/β-catenin signaling in vitro.

Cell Culture

The human HCC cell lines HepG2 and Huh7 were obtained from the American Type Culture Collection (Manassas, VA), propagated, and kept at the Yale Liver

Center (P30DK034989). To obtain conditioned medium (CM), the cells were grown to 80% confluence, washed twice with serum-free media, and then incubated with serum-free media overnight. The CM was obtained after 18–20 hours and was concentrated approximately 40-fold using Amicon Ultra centrifugal filters (Millipore, Billerica, MA) with a 10-kDa cutoff. For PEDF peptide experiments, the medium was removed, washed three times with serum medium, and PEDF 34-mer was added for 2 hours before the lysates were obtained. For the lysates, the cells were scraped in radioimmunoprecipitation assay buffer containing protease and phosphatase inhibitors, incubated on ice, and centrifuged at 10,000*g* for 10 minutes.

Silencing of PEDF and LRP6 With RNAi in Hepatocellular Carcinoma Cells

To reduce PEDF levels in human HCC cells, commercial small interfering RNA (siRNA) constructs targeting PEDF (cat. no. 4392420, 4390771) or scrambled (cat. no. 4390843) sequences (Ambion) were transfected according to the manufacturer's instructions. After 6 hours, the transfection medium was replaced with fresh medium lacking siRNA. After an additional 48 hours, the medium was changed to serum-free medium for 24 hours. CM and cell lysates were obtained as described earlier. The HepG2 cells stably transfected with small-hairpin RNA constructs targeting LRP6 were a gift of Dr. Arya Mani (Yale University School of Medicine). The integrity of PEDF and LRP6 KO was assessed in conditioned medium and in lysates. Measurement of PEDF levels in culture was performed with by a commercial enzyme-linked immunosorbent assay kit (Bio-Products, Frederick, MD).

RNA Analysis and Quantitative Polymerase Chain Reaction

The RNA was isolated using the RNAEasy mini kit (Qiagen). The primer probe sets were obtained from a commercial source (Applied Biosystems, Foster City, CA), and quantitative reverse-transcription PCR was performed on a TaqMan ABI 7500 system (Applied Biosystems) as described elsewhere.[13] Target gene expression was normalized against β-actin.

Immunoblotting

Immunoblotting was performed as described elsewhere.[12] Protein content was determined by Bradford assay. Lysates (20–30 μg total protein) were separated under denaturing conditions on a gradient gel (Bio-Rad Laboratories, Hercules, CA), and transferred to polyvinylidene fluoride membranes. After they were blocked in a 5% milk solution, the membranes were incubated overnight with antibodies. Primary antibodies used were PEDF from Chemicon (Temecula, CA); transforming growth factor-β1 (TGF-β1; 3711S), phospho-LRP6 (2568), total LRP6 (2560), nonphosphorylated (active) β-catenin and total β-catenin, phospho-glycogen synthase kinase-3β (p-GSK3β), total GSK3β, phospho-extracellular-signal-regulated kinase (p-ERK), total ERK (4370), and glyceraldehyde-3-phosphate dehydrogenase (GAPDH) (5174S) from Cell Signaling Technology (Beverly, MA); collagen I (ab6308) from Abcam (Cambridge, MA); collagen III (15946) from Novus

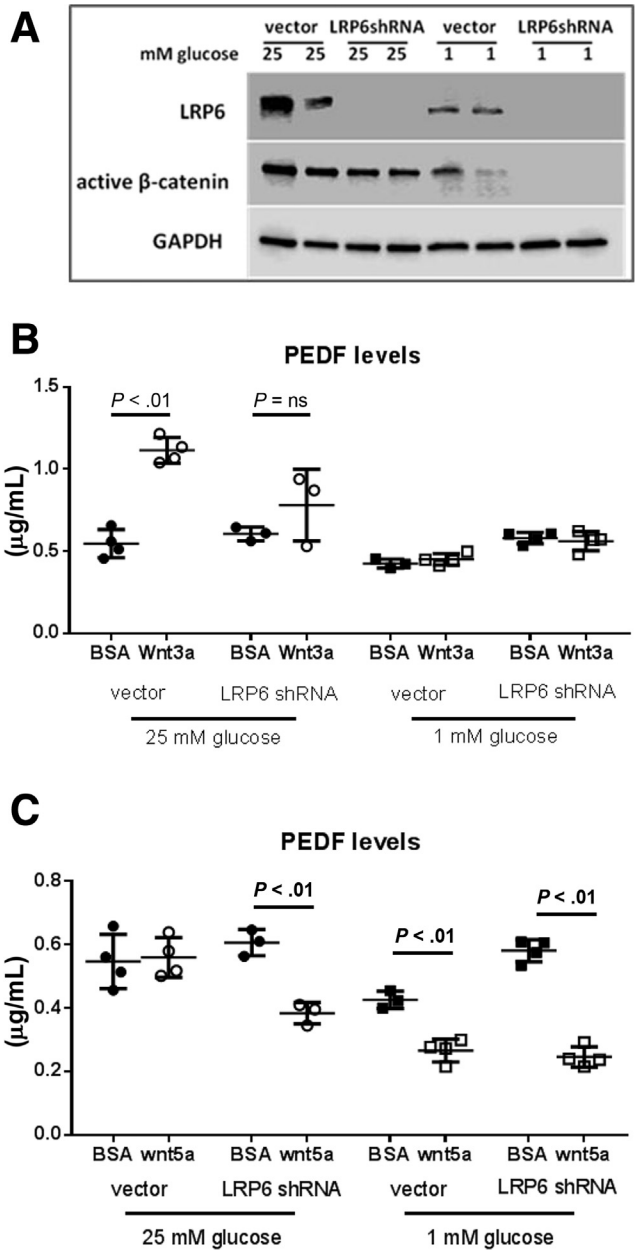

Figure 1. PEDF secretion is regulated by Wnt ligands in an LRP6-dependent manner. (*A*) Integrity of the LRP6 small-hairpin RNA-mediated knockdown in HepG2 cells was demonstrated under high (25 mM) and low (1 mM) glucose conditions. (*B*) Canonical Wnt3a ligand significantly induces PEDF levels in the presence of the Wnt coreceptor LRP6 ($P < .01$). Genetic knockdown of LRP6 or its functional depletion with 1 mM glucose abrogates this effect (not statistically significant). (*C*) The noncanonical Wnt5a suppresses PEDF levels when LRP6 is genetically deleted under 25 mM glucose or reduced by low glucose ($P < .01$). Experiments were conducted in duplicate with n = 3–4/group. Data are presented as mean ± SD.

Biologicals (Oakville, ON, Canada); and β-actin from Sigma-Aldrich.

Collagen I blots were run under reducing and nonreducing conditions. After washing in Tris-buffered saline and 0.05% Tween, the primary antibody was labeled using a peroxidase-conjugated secondary antibody specific for the primary antibody species. Samples were resolved on a gradient gel and transferred to nitrocellulose membranes. Equivalence of loading was confirmed using β-actin or GAPDH for lysates, or Coomassie stains for CM. Densitometry was performed using the National Institutes of Health ImageJ software (http://imagej.nih.gov/ij/).

Hydroxyproline Assays

Hydroxyproline assays were performed using a commercial kit (BioVision Research, Mountain View, CA). Measurements were performed on four separate occasions using three different sets (n = 3–4/group) of age-matched PEDF KO and control livers.

Second Harmonic Generation Imaging

Second harmonic generation (SHG) imaging preferentially detects type I, and to a lesser extent type III, fibrillar collagen.[26] Multiphoton stimulation combined with tissue clearing was used to visualize fibrillar collagen deposition in volume sections of both WT and KO liver specimens measuring approximately 5 × 5 × 1 mm. Tissue clearing was performed on formalin-fixed organs using benzyl alcohol/benzyl benzoate (BABB) in 2:1 ratio as previously described elsewhere.[27] Briefly, tissue specimens were then dehydrated by graded methanol incubations in 30-minute intervals and then incubated overnight with BABB. SHG was measured on a TriM Scope II multiphoton microscope (LaVision BioTec, Bielefeld, Germany) with 780 nm excitation and 390 nm band pass emission filter using a 0.95 NA, 25× objective (Leica Microsystems GmbH, Wetzlar, Germany) designed specifically for BABB immersion. Tissue volume was determined using intrinsic fluorescence with 960 nm excitation and 600–50 nm band pass filter detection. The SHG signal was collected in reflection: the specimen was placed on a deep-well slide, and a mirror was placed underneath to improve collection efficiency. The imaging parameters were kept constant among the specimens, including laser power and scanning speed as well as detector distance from the specimen. Data were collected in 16-bit depth, and contrast was adjusted using identical intensity thresholds for all images, allowing for direct intensity comparison.

Histology

Immunohistochemical analysis was performed as described on 14 sequentially obtained human HCC specimens. Sections were deparaffinized, treated to inhibit endogenous peroxidase, and subjected to antigen retrieval. After incubation with primary antibody, sections were washed and then incubated with biotinylated anti-mouse antiserum. Streptavidin complexed with horseradish peroxidase was added, and labeling was detected using diaminobenzidine. Semiquantitative scoring of the immunohistochemical labeling was evaluated by a pathologist (S.E.C.) using a numerical grading score (1, no staining; 2, focal positivity; 3, moderate; 4, diffuse, strong immunostaining) on 10 nonoverlapping fields per case with normal hepatocytes distant to the tumor margin assessed as "Nl liver."

Statistical Analysis

The *P* values were calculated, assuming equal sample variance, using a two-tailed Student *t* test on Prism software. $P < .05$ was considered statistically significant. Values were stated as mean ± standard deviation (SD) or standard error of the mean.

Results

PEDF Secretion Is Wnt3a-Responsive and Depends on the Wnt Coreceptor LRP6

We evaluated PEDF regulation by Wnt ligands and dependence upon LRP6. The integrity of the LRP6 KO and the stimulatory effects of high (25 mM) versus low (1 mM) glucose on LRP6 and its effector active (nonphosphorylated) β-catenin were shown (Figure 1*A*). Canonical Wnt3a (50 ng/mL) led to a greater than twofold increase in PEDF levels that was LRP6 dependent (Figure 1*B*, $P < .01$). In the absence of the LRP6, Wnt3a had no effect on PEDF levels. Similarly, Wnt3a had no effect on PEDF levels under 1 mM glucose conditions, likely reflecting markedly suppressed LRP6 levels seen in this condition. Thus, Wnt3a-stimulated induction of PEDF levels are LRP6 dependent.

The noncanonical Wnt pathway includes the Wnt5a ligand and its orphan receptor, ROR2 (receptor tyrosine kinase-like orphan receptor 2), and counters the effects of the canonical pathway.[28] To determine whether PEDF could be modulated by the noncanonical pathway, Wnt5a was added to HepG2 cells with and without LRP6. Wnt5a did not alter PEDF levels under high-glucose conditions in the presence of the LRP6 receptor. When the canonical receptor LRP6 was deleted, Wnt5a significantly suppressed PEDF protein levels (Figure 1*C*, $P < .01$). Thus, deletion of LRP6 favors the noncanonical pathway and lowers PEDF under high-glucose conditions.

Similarly, the 1 mM glucose condition leads to a functional depletion of the LRP6 receptor (Figure 1*A*) without genetic manipulation. Here, the Wnt5a ligand significantly decreased PEDF under scrambled and LRP6 KO conditions indicating that the noncanonical Wnt ligands can decrease PEDF in the setting of diminished LRP6 levels (Figure 1*C*, $P < .01$ for low glucose with and without LRP6). Thus, canonical Wnt3a and the noncanonical Wnt5a differentially regulate PEDF levels.

PEDF Knockout Livers Resemble Experimental and Human Hepatocellular Carcinoma Marked by Wnt/β-Catenin Signaling

To explore PEDF's role in the liver, gene expression profiling was done in KO versus WT livers. There were 1113

Table 1. Top 10 Enriched Chemical and Genetic Perturbation Gene Sets Corresponding to PEDF Null Livers

Gene Set Name	FDR *q* Value[a]	Gene Set Description
LEE_LIVER_CANCER_ACOX1_UP	<.001	Genes up-regulated in HCC of ACOX1 knockout mice
LEE_LIVER_CANCER_E2F1_UP	<.001	Genes up-regulated in HCC induced by overexpression of E2F1
LEE_LIVER_CANCER_MYC_E2F1_UP	<.001	Genes up-regulated in HCC from MYC and E2F1 double transgenic mice
LEE_LIVER_CANCER_MYC_TGFA_UP	<.001	Genes up-regulated in HCC tissue of MYC and TGFA double transgenic mice
ICHIBA_GRAFT_VERSUS_HOST_DISEASE_35D_UP	<.001	Hepatic graft versus host disease day 35: genes up-regulated in allogeneic vs syngeneic bone marrow transplant
KHETCHOUMIAN_TRIM24_TARGETS_UP	<.001	Retinoic acid-responsive genes up-regulated in HCC samples of TRIM24 knockout mice
LEE_LIVER_CANCER_CIPROFIBRATE_UP	<.001	Genes up-regulated in HCC induced by ciprofibrate
LEE_LIVER_CANCER_DENA_UP	<.001	Genes up-regulated in HCC induced by diethylnitrosamine
WIELAND_UP_BY_HBV_INFECTION	<.001	Genes induced in the liver during hepatitis B viral clearance in chimpanzees
BORLAK_LIVER_CANCER_EGF_UP	<.001	Genes up-regulated in HCC developed by transgenic mice overexpressing a secreted form of epidermal growth factor in liver

Note: Gene set enrichment analysis showed that expression signatures in PEDF knockout mouse livers resembled those found in genetic and chemical models of HCC. Of the top 10 enriched chemical and genetic perturbation gene sets, eight represented rodent models of HCC, and two (Ichiba and Wieland) sets are related to inflammatory liver conditions. HCC, hepatocellular carcinoma.
[a]FDR (false-discovery rate): adjusted *P* value (FDR *q* value).

gene entities differentially expressed between WT and KO animals at FDR $\leq$ .05 and 1.3-fold expression cutoffs. Out of 1113 genes 344 were up-regulated in KOs, and 769 were down-regulated (Supplementary Table 1). Grouping these genes by GO categories using hypergeometric model showed that most up-regulated GO categories were related to extracellular matrix function, lipid metabolism, immune response, DNA replication, phase I and II enzymes (FDR $\leq$ .05). Most down-regulated GO categories were related to ribosomal and mitochondrial function and numerous

Table 2. Up-Regulated Gene Sets From PEDF KO Livers Matching Gene Expression Signatures Associated With Aberrant Wnt/β-Catenin Signaling

Name	FDR[a]	Description, Web Link, and PubMed ID
HOSHIDA LIVER CANCER SUBCLASS S1	<.001	Gene signature from HCC subset with aberrant Wnt activation http://www.broadinstitute.org/gsea/msigdb/cards/HOSHIDA_LIVER_CANCER_SUBCLASS_S1 PUBMED ID: 19723656
KENNY CTNNB1 TARGETS UP	.002	Genes up-regulated in mammary epithelial cells with constitutively active mutant β-catenin gene http://www.broadinstitute.org/gsea/msigdb/cards/KENNY_CTNNB1_TARGETS_UP.html PUBMED ID: 15642117
CAVARD LIVER CANCER MALIGNANT VS BENIGN	.003	Genes identified by subtractive hybridization to compare gene expression between malignant and benign components of a human HCC occurring from pre-existing adenoma with activated β-catenin http://www.broadinstitute.org/gsea/msigdb/cards/CAVARD_LIVER_CANCER_MALIGNANT_VS_BENIGN.html PUBMED ID: 16314847
CHIANG LIVER CANCER SUBCLASS CTNNB1 UP	.031	Genes up-regulated in the subclass of HCC characterized by activated β-catenin (*CTNNB1*) gene http://www.broadinstitute.org/gsea/msigdb/cards/CHIANG_LIVER_CANCER_SUBCLASS_CTNNB1_UP.html PUBMED ID: 18701503
CAIRO HEPATOBLASTOMA UP	.050	Gene signature from human hepatoblastoma characterized by Wnt/β-catenin activation http://www.broadinstitute.org/gsea/msigdb/cards/CAIRO_HEPATOBLASTOMA_UP.html PUBMED ID: 19061838

[a]FDR (false-discovery rate): adjusted *P* value (FDR *q* value).

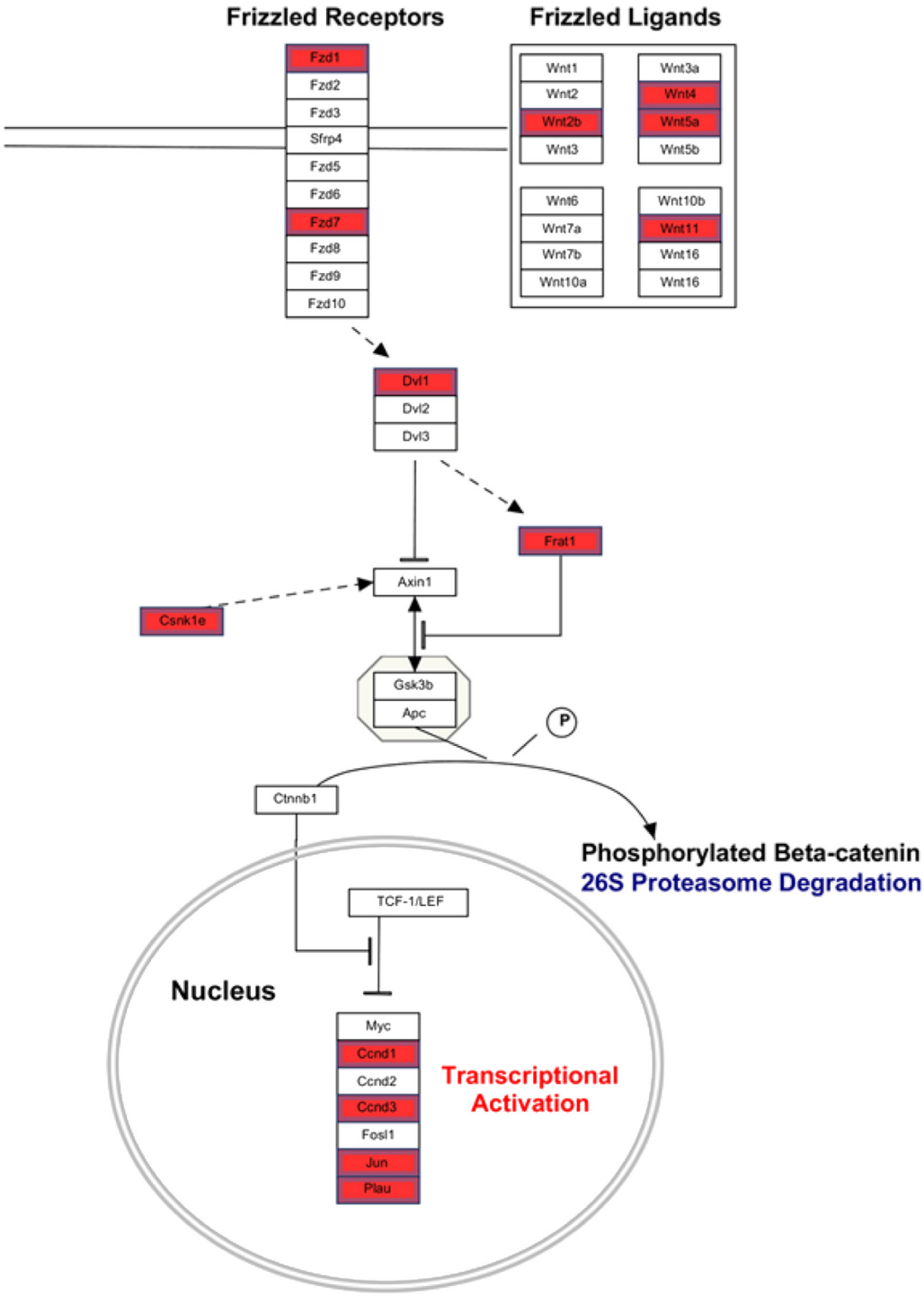

Figure 2. Expression profiling of PEDF knockout (KO) livers demonstrates up-regulation of genes involved in Wnt/β-catenin signaling. Items in red represent genes that were up-regulated <1.1-fold in PEDF KO compared with wild-type (WT) livers. In particular, Frizzled ligands known to play a role in hepatocarcinogenesis were up-regulated. Induction of multiple downstream targets of Wnt/β-catenin (*Ccnd1*, *Ccnd3*, *Jun*, and *Plau*) suggests transcriptional activation of Wnt/β-catenin signaling.

primary metabolic processes such as nitrogen compound metabolism, glutamine family amino acid metabolic process, urea cycle, and carboxylic acid metabolism, and peptidase inhibitory activity (FDR $<$ .05).

To further characterize the gene expression changes in KO mice, GSEA using curated pathways as well as GO categories were performed. Consistent with analysis by moderated *t* test, the GSEA showed that most up-regulated

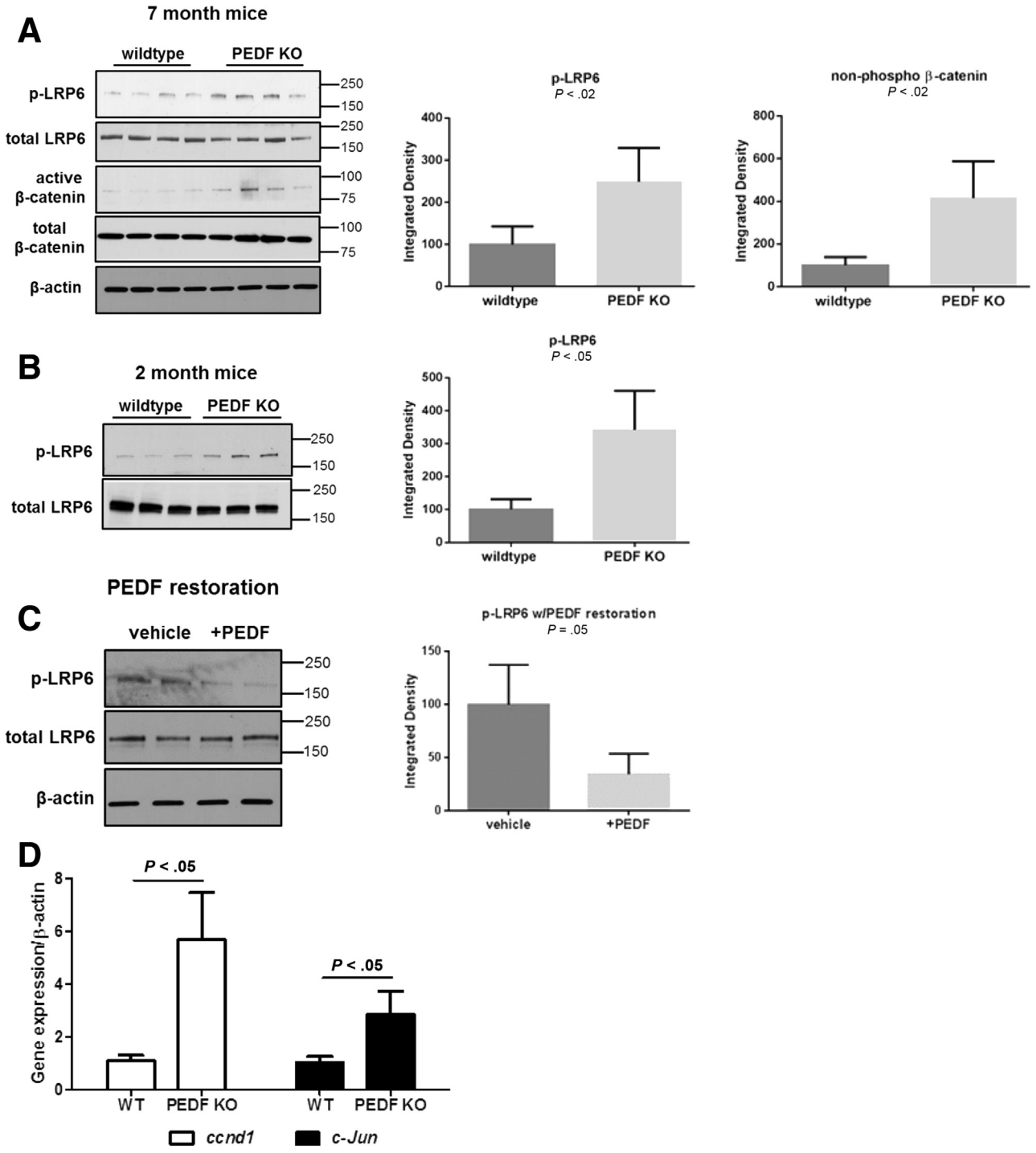

Figure 3. PEDF inhibits LRP6 phosphorylation in murine livers. (*A*) Increased phospho-LRP6 and nonphosphorylated (active) β-catenin in 7-month-old PEDF knockout (KO) mice and corresponding quantification of immunoblots ($P < .02$). (*B*) Younger 2 month-old) PEDF KO mice also show increased phosphorylation of LRP6 ($P < .05$). (*C*) PEDF restoration in vivo reduces LRP6 activation ($P = .05$). (*D*) Gene expression of *Ccnd1* and *c-Jun* in murine control and PEDF KO livers. Representative data from duplicate experiments conducted with n = 3–4/group for immunoblots. Quantitative reverse-transcription polymerase chain reaction data, n = 6/group. Data are presented as mean ± SD.

pathways were related to cell proliferation, inflammatory responses, collagen expression, extracellular matrix function, and phase I and phase II enzymatic activity (Supplementary Table 2). Subsequently, another GSEA was performed to test for similarities between gene expression profiles in PEDF KO mouse livers and curated gene sets representing expression signatures of genetic and chemical perturbation. This analysis showed that the most significantly enriched gene sets represented rodent models and human samples of HCC tissues and various

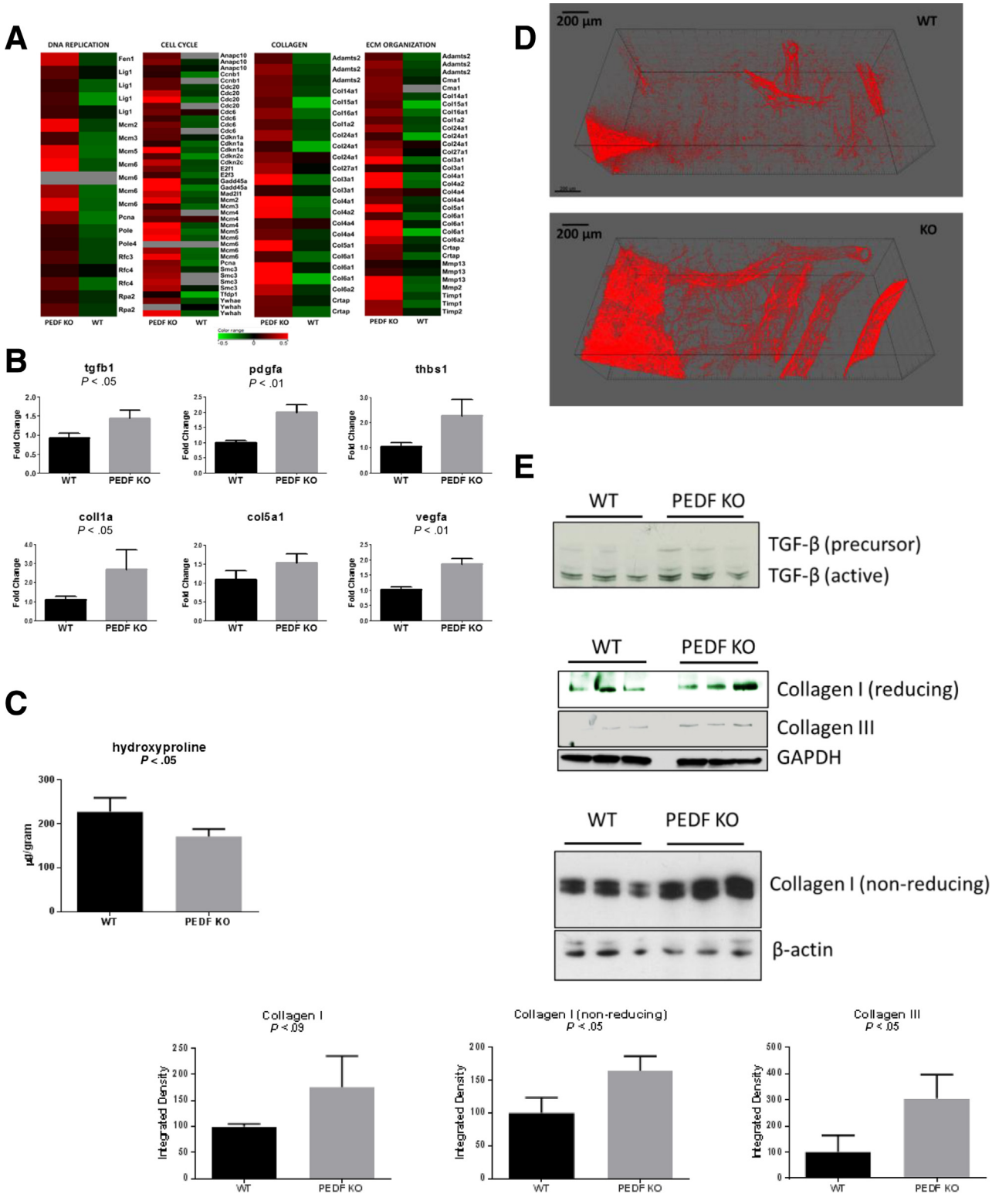

inflammatory liver conditions, suggesting that loss of PEDF leads to gene expression changes similar to those found in HCC (Table 1, Supplementary Table 3). In fact, eight out of top 10 enriched gene sets represented rodent models of HCC (Table 1).

PEDF Knockout Livers Display a Genomic Signature Resembling Hepatocellular Carcinoma Categorized by Wnt/β-Catenin Signaling

Comparison of liver-specific gene expression signatures of genetic and chemical perturbation to PEDF KO livers

showed a striking resemblance to various human HCC subsets marked by overactive Wnt/β-catenin signaling (Table 2).[3,29–31] Furthermore, PEDF KO liver expression profiles also correlated with the gene expression patterns of nonliver tissue experimental models where constitutively active mutant β-catenin was overexpressed (Table 2).[32] Additionally, we observed overexpression of both Fzd 1 and 7, Wnt coreceptors that have been reported to be induced in human HCC specimens and cell lines (Figure 2).[33] Downstream targets of Wnt/β-catenin signaling, such as *Ccnd1*, *Ccnd3*, and *c-Jun*, were also found to be up-regulated in PEDF KO livers.

PEDF Inhibits Activation of the Wnt Coreceptor LRP6 In Vivo

To evaluate concordance with the genomic analysis, we interrogated components of the Wnt/β-catenin signaling pathway in PEDF KO livers before and after PEDF reconstitution. PEDF KO livers showed enhanced phospho-LRP6 levels and active β-catenin compared with WT controls in 7-month-old mice (Figure 3*A*, $P < .02$). A similar activation of LRP6 was seen in 2-month-old mice (Figure 3*B*, $P < .05$). Restoration of PEDF in KO mice resulted in decreased LRP6 phosphorylation without affecting total LRP6 levels (Figure 3*C*, $P = .05$). Moreover, gene expression of downstream canonical Wnt signaling pathway targets *Ccnd1* and *c-Jun* was increased in PEDF KO livers versus controls (Figure 3*D*, $P < .05$). These results indicate that PEDF functions as an antagonist of hepatic LRP6 activation in vivo and that exogenous PEDF can inhibit LRP6 activation in vivo.

PEDF Loss Is Associated With Increased Fibrogenic Markers and Enhanced Cellular Proliferation

PEDF expression is reduced in human cirrhosis, and its restoration in two different models of experimental liver cirrhosis mitigates fibrotic changes.[14,16] Consistent with this finding, the GSEA revealed an induction of pathways related to extracellular matrix deposition in PEDF KO liver tissue (Figure 4*A*, Supplementary Table 1). Biochemical assessment of collagen content and specific collagen subtypes, however, revealed a more complex picture of the matricellular changes in the absence of PEDF.

Confirmation of fibrogenic cytokines with quantitative PCR showed that *tgfb1* and *pdgfa* were significantly increased, and *thbs1*, an activator of transforming growth factor-β, showed a trend toward increased expression (Figure 4*B*). Angiogenic factors play a role in promoting fibrogenesis and can be regulated by Wnt pathway activation.[34] Enhanced expression of *vegfa* was present in PEDF KO livers (Figure 4*B*). Similarly, expression of *col1a* was increased but not that of other fibrillar collagen types such as *col5a*1. Surprisingly, the total hydroxyproline content of PEDF KO livers was 75% of the control livers (Figure 4*C*), indicating that overall the collagen content was decreased. However, SHG imaging revealed visual evidence of increased fibrillar collagen in PEDF KO livers (Figure 4*D*). Consistent with the SHG imaging, the fibrillar collagen types I and III levels in PEDF KO livers were higher than in the controls (Figure 4*E*). Thus, a preferential induction of fibrillar collagen occurs in PEDF KO livers, but it is accompanied by an overall decrease in other collagen or structural proteins that contain hydroxyproline residues.

PEDF Is a Secreted Antagonist of Wnt/β-Catenin Signaling in Hepatocellular Carcinoma Cells

Findings in murine livers were extended to human HCC cells to determine whether PEDF functions as a Wnt antagonist. Both HepG2 and Huh7 cells secreted PEDF into the CM (Figure 5*A* and *C*). In HepG2 cells, siRNA-mediated PEDF knockdown led to increased phospho-LRP6 and active β-catenin levels (Figure 5*A* and *B*, $P < .01$). Similar results were observed in Huh-7 cells after PEDF knockdown (Figure 5*C* and *D*, $P < .01$).

A 34-mer sequence within PEDF mediates its well-documented antiangiogenic effects.[25] Because angiogenesis requires Wnt signaling, we surmised that the PEDF 34-mer is responsible for its effects on Wnt/β-catenin signaling. Adding the PEDF 34-mer decreased the levels of active phospho-LRP6 and active β-catenin (Figure 5*E*, $P < .01$). Downstream regulators and targets of Wnt signaling such as GSK3β and phospho-ERK levels corresponded to the effects of Wnt blockade with PEDF 34-mer (Figure 5*F*). Levels of phospho-GSK3β (inactive form) were diminished consistent with increased intracellular active GSK3β and enhanced degradation of β-catenin seen with Wnt blockade. The downstream targets of β-catenin such as phospho-ERK were decreased. Moreover, transcriptional targets of canonical Wnt signaling such as *ccnd1* and *c-Jun* were suppressed with the 34-mer (Figure 5*G*). These results demonstrate that PEDF antagonizes Wnt/β-catenin signaling in human HCC

Figure 4. (***See previous page***). **Absence of PEDF is permissive for induction of fibrogenic markers.** (*A*) Gene expression heat maps show up-regulation of DNA replication, collagen, and extracellular matrix organization pathways. Heat maps represent graphic gene expressions of the genes contributing most to statistically significant enrichment score in gene set enrichment analysis (core enriched genes). The log transformed color expression scale is shown at the bottom of the figure. (*B*) PEDF KO livers demonstrate enhanced expression of profibrotic cytokines (*tgfb1*, $P < .05$; *pdgfa*, $P < .01$, *vegfa*, $P < .01$) and fibrillar collagen. (*C*) Decreased hydroxyproline in PEDF KO livers. (*D*) Second harmonic generation (SHG) imaging demonstrates enhanced fibrillar collagen deposition adjacent to vessels in PEDF KO livers. (*E*) Transforming growth factor-β (TGF-β) and fibrillar type I and III collagens were increased in PEDF KO livers under reducing and nonreducing conditions. Quantitative reverse-transcription polymerase chain reaction data, n = 5–6/group; data are presented as mean ± S.E.M. Representative SHG images taken from n = 3/group. Representative hydroxyproline data from n = 4 separate experiments from three different sets of age-matched livers; data are presented as mean ± SD. Immunoblots are from n = 3 livers/group from three separate experiments; data are presented as mean ± SD.

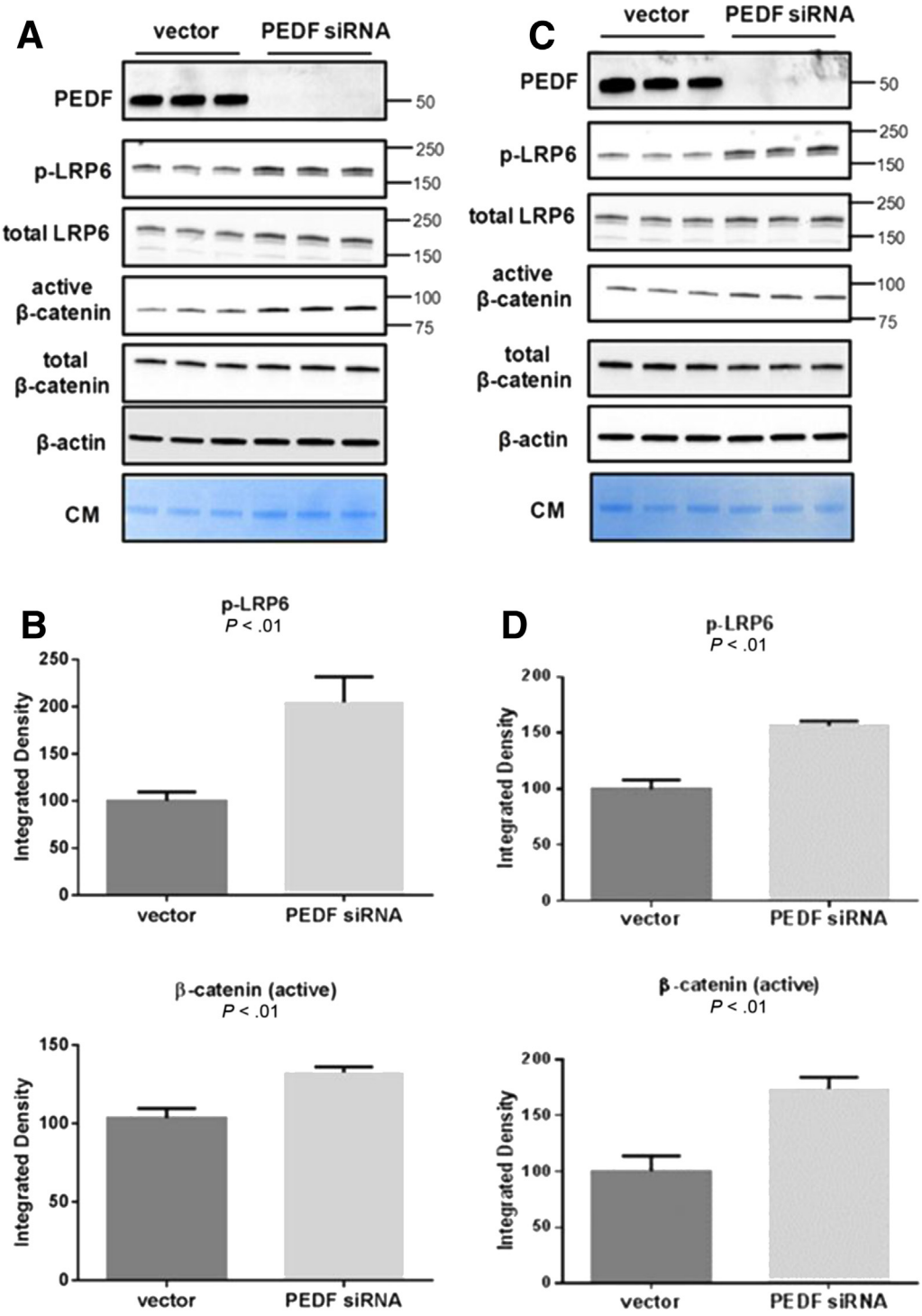

Figure 5. PEDF inhibits canonical Wnt/β-catenin signaling in human hepatocellular carcinoma (HCC) cells. (*A*) PEDF knockdown in HepG2 cells results in increased LRP6 phosphorylation and increased active β-catenin. (*B*) Corresponding quantification of phospho-LRP6 and active β-catenin after RNA interference of PEDF in HepG2 cells ($P < .01$). (*C*) Huh-7 cells display increased LRP6 phosphorylation and active β-catenin after depletion of endogenous PEDF. (*D*) Quantification of phospho-LRP6 and active β-catenin after RNA interference of PEDF in Huh-7 cells ($P < .01$). (*E*) A PEDF 34-mer peptide decreased LRP6 phosphorylation and active β-catenin levels in Huh-7 cells ($P < .01$). (*F*) Changes in the levels of downstream targets of canonical Wnt signaling such as phospho-GSK3β/total GSK3β and phospho-ERK/total ERK reflect inhibition of Wnt signaling with the PEDF 34-mer. (*G*) Gene targets of the Wnt pathway, *ccnd1* and *c-Jun,* were significantly suppressed with PEDF 34-mer ($P < .05$ and $P < .01$, respectively). Representative data are shown from three separate experiments conducted with n = 3/group for siRNA experiments. Data from 34-mer peptide experiments were performed in duplicate and n = 3/group. Data are presented as mean ± SD.

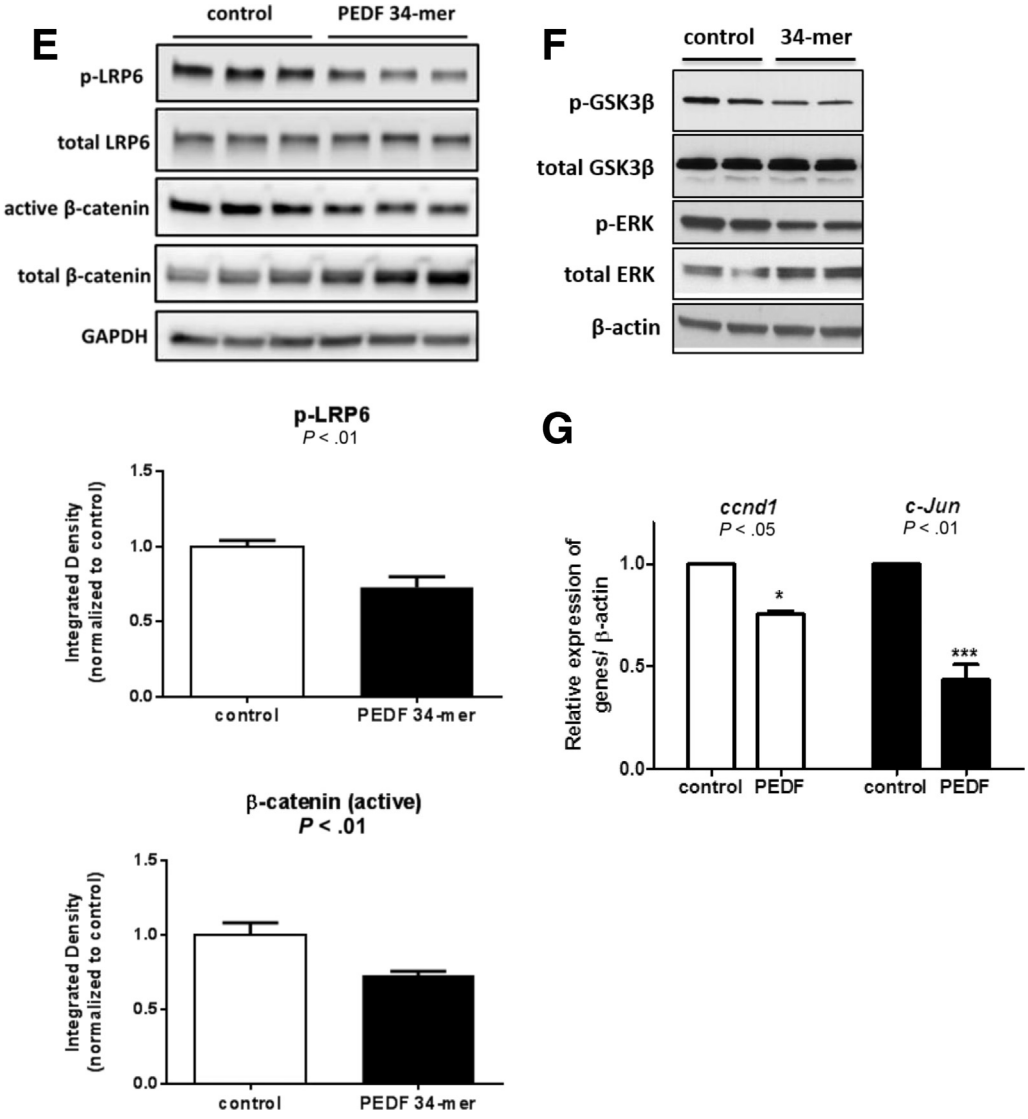

Figure 5. (*continued*).

cells and point to a 34-amino-acid peptide fragment derived from PEDF that mediates LRP6 blockade.

Induction of Liver Fibrosis and Sporadic Hepatocellular Carcinoma in PEDF Knockout Mice After Western Diet Feeding

Genomic profiling of PEDF KO livers corresponded to various human HCC subsets marked by overactive Wnt/β-catenin, but spontaneous HCC did not develop in PEDF KO mice up to 1 year of age (data not shown). To test whether diet-induced obesity could induce HCC formation in the absence of PEDF, a Western diet (40% fat, 44% carbohydrate, 16% protein) was given to PEDF KO and WT mice for 6 to 8 months. A Western diet increased fibrosis in WT and PEDF KO mice as shown by trichrome staining and hydroxyproline measurements (Figure 6*A*).

Increased fibrillar collagen deposition as seen with SHG imaging was more apparent in PEDF KO than WT livers (Figure 6*B*). Three-dimensional reconstructed images from SHG imaging revealed an increase in fibrillar collagen adjacent to vessels, outlining their structures (Figure 6*B*). A subset of PEDF KO mice (3 of 12) developed macroscopic tumor formation compared with none (0 of 12) in the control mice (Figure 6*C*) after chronic Western diet feeding. Histologic examination showed features consistent with a well-differentiated HCC with the increased presence of unpaired blood vessels (Figure 6*C*, *arrows*). In contrast to the diet-induced HCC, a one-time diethylnitrosamine injection did not result in HCC formation in either the WT or KO mice at 6 months (data not shown). Thus, PEDF deficiency combined with a chronic Western diet led to sporadic HCC formation.

PEDF Expression Is Reduced in Human Hepatocellular Carcinoma Specimens

A previous study of embryonic and adult human tissue sites demonstrated that the liver has the highest

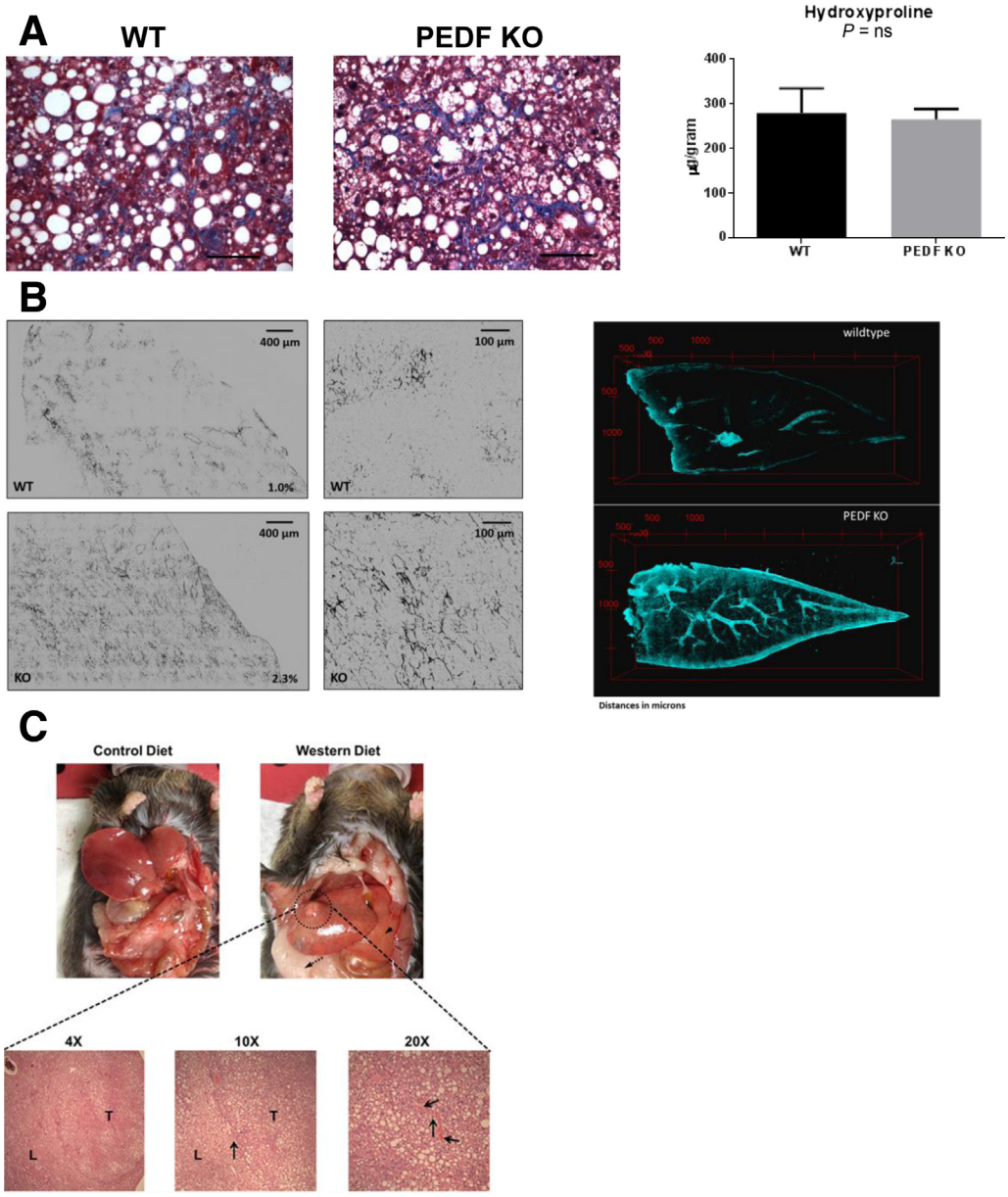

Figure 6. A Western diet induces liver fibrosis and sporadic hepatocellular carcinoma (HCC) in PEDF knockout (KO) mice. (*A*) Six months of Western diet feeding induced liver fibrosis in wild-type (WT) and PEDF KO mice as demonstrated by trichrome staining (magnification 20×; size bars: 100 μM) and measured by hydroxyproline content. (*B*) Second harmonic generation (SHG) imaging shows increased fibrillar type I/III collagen deposition in PEDF KO mice livers (*bottom panels*) compared with WT (*top panels*) mice fed a Western diet. Magnification: *left* 4×; *right* 20×. Three-dimensional reconstruction of serial SHG images reveals prominence of fibrillar collagen around blood vessels in PEDF KO livers. (*C*) PEDF KO mice showing macroscopic tumor in mice fed the Western diet versus control diet. Bottom panel shows histology of a well-differentiated HCC arising in KO mouse fed a Western diet. L, liver; T, tumor; magnification 10×, arrow at demarcation between liver and HCC; 20×, arrows highlighting unpaired blood vessels in HCC.

expression levels of the PEDF gene, and the recent tissue-based map of the human proteome confirmed this finding.[20,21] Relative to the high endogenous levels in the normal liver, we asked whether PEDF levels in HCC specimens were diminished. Staining of PEDF showed diffuse and strong immunoreactivity for PEDF in normal liver tissue (Figure 7*A*, *left).* In contrast, PEDF immunolabeling was statistically significantly reduced in HCC compared with the adjacent liver (Figure 7*A*, *middle* and *right,* and *B*; $P < .01$). Thus, human HCC specimens demonstrated decreased PEDF expression compared with the adjacent nontransformed hepatocytes.

Discussion

Aberrant Wnt/β-catenin signaling underlies a number of malignancies, including HCC.[3,35] Our study has identified PEDF as an endogenous inhibitor of LRP6 activation that is

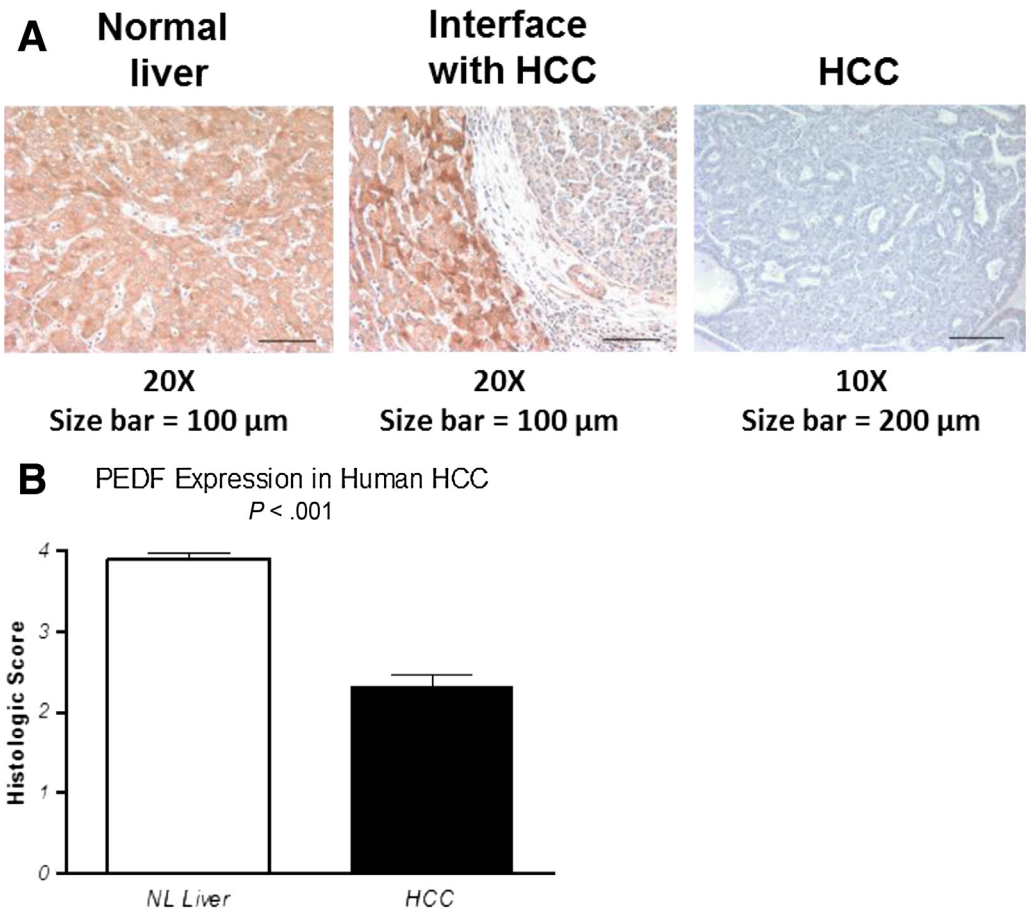

Figure 7. PEDF expression is reduced in human hepatocellular carcinoma (HCC). (*A*) Immunostaining for PEDF in human livers (*top*) and human HCC specimens (*bottom*). (*B*) Semiquantitative scoring of PEDF staining demonstrates increased labeling in normal liver compared with HCC specimens ($P < .01$; $n = 14$). NL, normal.

secreted in response to canonical Wnt ligands. Enhanced LRP6 and β-catenin activation was seen in the livers of PEDF KO mice and in two human HCC cell lines where PEDF was depleted. Further, adding a PEDF 34-mer inhibited LRP6, active β-catenin, and downstream targets of Wnt signaling, thereby identifying the region on PEDF that mediates Wnt inhibitory effects. These data support the idea that PEDF functions as a part of a negative feedback loop to modulate Wnt signaling. Gene enrichment data supported this interaction. Further, biochemical analyses of PEDF KO murine livers before and after PEDF reconstitution in vivo confirmed that PEDF can block Wnt signaling in the liver. PEDF knockdown in two human HCC cell lines led to increased Wnt/β-catenin signal transduction with a specific 34-amino-acid region mediating these effects. Thus, PEDF is regulated by and inhibits the canonical Wnt/β-catenin pathway in the murine liver and in two human HCC cell lines.

The genomic analysis in this study correlated with genetic profiles of murine hepatocarcinogenesis and human HCC subsets marked by overactive Wnt/β-catenin signaling, but PEDF deficiency alone did not result in HCC formation. A prolonged nutritional challenge induced only a fraction of animals to develop a well-differentiated HCC. These results are consistent with models of hepatic overexpression of normal and mutant β-catenin that do not result in spontaneous HCC.[35] Paradoxically, deletion of β-catenin from the liver is permissive for HCC formation after injection with diethylnitrosamine.[36] This surprising effect of β-catenin deletion conferring an increased rate of HCC development in murine models, rather than its overexpression, reflects the importance of this pathway for liver tissue homeostasis. In its absence, the liver is prone to injury from oxidative stress and enhanced fibrosis.[36] Thus, findings from β-catenin transgenic mice are at odds with those from genomic and immunohistochemical studies in human HCC, which point to Wnt/β-catenin signaling as a significant driver in a subset of HCC.[3] The absence of HCC found in transgenic models of β-catenin overexpression and the occurrence of HCC with β-catenin deletion highlights the limitations of constitutively active or deletion of β-catenin, where temporal and context-specific activity of β-catenin may more accurately capture its role in human disease.

Absence of PEDF led to complex changes to the ECM of the liver. Despite lower total hydroxyproline levels, type I/III collagen content and SHG imaging demonstrated increased deposition of fibrillar collagen in PEDF KO livers. In experimental and human cirrhosis specimens, PEDF levels are also depleted.[14] Restoration of PEDF in

experimental models of CCl_4 [chemokine (C-C motif) ligand 4] and bile-duct ligated cirrhosis ameliorates tissue fibrosis, suggesting an important role for endogenous PEDF in maintaining quiescence of the liver ECM.[14,16] These findings are consistent with studies that demonstrate Wnt/β-catenin signaling as a regulator of the fibrotic response in diverse organs.[37–39] Further, examination of the PEDF null state in humans, osteogenesis imperfecta type VI, points to abnormalities in the extracellular matrix.[24,40] These findings suggest that PEDF may regulate matricellular content in multiple organ sites.

This study provides further evidence to support the role of PEDF in Wnt/β-catenin signaling. The discovery through exome sequencing that null mutations in PEDF cause osteogenesis imperfecta type VI implicated PEDF's role in modulating Wnt/β-catenin signaling in human disease.[22,40,41] We and others have shown that PEDF could induce differentiation of progenitor cells and that these effects were LRP6 dependent.[22,42] In the eye, PEDF inhibited Wnt3a-mediated β-catenin nuclear translocation, and recent studies showed that PEDF directly suppressed other Wnt modulators such as sclerostin.[19,41] Exogenous PEDF protein and a peptide derived from PEDF demonstrate inhibitory effects on Wnt signaling in the liver and in two HCC cell lines, thereby pointing to its role in attenuating Wnt signaling in a negative feedback loop.

Interestingly, PEDF appears to promote Wnt/β-catenin signaling in stem cell populations but inhibits Wnt signaling in differentiated cells.[22,41] Differential effects are also seen in Wnt ligands and Wnt-related proteins such as Wnt5a and Dickkopf2, and stem from selective expression patterns of Wnt coreceptors.[28,43,44] Future studies detailing the expression patterns of different Fzd species should allow identification of the receptor combination that directs PEDF's different functional outcomes as they pertain to Wnt signaling.

In summary, PEDF functions as an endogenous inhibitor of Wnt/β-catenin signaling in the liver and in human HCC cells. These findings provide a framework for understanding the antitumor properties of PEDF in other cancer types.

References

1. El-Serag HB. Hepatocellular carcinoma. N Engl J Med 2011;365:1118–1127.
2. Lee JS, Chu IS, Heo J, et al. Classification and prediction of survival in hepatocellular carcinoma by gene expression profiling. Hepatology 2004;40:667–676.
3. Hoshida Y, Nijman SM, Kobayashi M, et al. Integrative transcriptome analysis reveals common molecular subclasses of human hepatocellular carcinoma. Cancer Res 2009;69:7385–7392.
4. Hoshida Y, Villanueva A, Kobayashi M, et al. Gene expression in fixed tissues and outcome in hepatocellular carcinoma. N Engl J Med 2008;359:1995–2004.
5. Tsuchiya M, Parker JS, Kono H, et al. Gene expression in nontumoral liver tissue and recurrence-free survival in hepatitis C virus-positive hepatocellular carcinoma. Mol Cancer 2010;9:74.
6. Chiodoni C, Colombo MP, Sangaletti S. Matricellular proteins: from homeostasis to inflammation, cancer, and metastasis. Cancer Metastasis Rev 2010;29:295–307.
7. Yasui N, Mori T, Morito D, et al. Dual-site recognition of different extracellular matrix components by anti-angiogenic/neurotrophic serpin, PEDF. Biochemistry 2003;42:3160–3167.
8. Uehara H, Miyamoto M, Kato K, et al. Expression of pigment epithelium-derived factor decreases liver metastasis and correlates with favorable prognosis for patients with ductal pancreatic adenocarcinoma. Cancer Res 2004;64:3533–3537.
9. Fitzgerald DP, Subramanian P, Deshpande M, et al. Opposing effects of pigment epithelium-derived factor on breast cancer cell versus neuronal survival: implication for brain metastasis and metastasis-induced brain damage. Cancer Res 2012;72:144–153.
10. Becerra SP, Notario V. The effects of PEDF on cancer biology: mechanisms of action and therapeutic potential. Nat Rev Cancer 2013;13:258–271.
11. Doll JA, Stellmach VM, Bouck NP, et al. Pigment epithelium-derived factor regulates the vasculature and mass of the prostate and pancreas. Nat Med 2003; 9:774–780.
12. Chung C, Shugrue C, Nagar A, et al. Ethanol exposure depletes hepatic pigment epithelium-derived factor, a novel lipid regulator. Gastroenterology 2009; 136:331–340.e2.
13. Schmitz JC, Protiva P, Gattu AK, et al. Pigment epithelium-derived factor regulates early pancreatic fibrotic responses and suppresses the profibrotic cytokine thrombospondin-1. Am J Pathol 2011;179:2990–2999.
14. Ho TC, Chen SL, Shih SC, et al. Pigment epithelium-derived factor is an intrinsic antifibrosis factor targeting hepatic stellate cells. Am J Pathol 2010;177: 1798–1811.
15. Grippo PJ, Fitchev PS, Bentrem DJ, et al. Concurrent PEDF deficiency and Kras mutation induce invasive pancreatic cancer and adipose-rich stroma in mice. Gut 2012;61:1454–1464.
16. Mejias M, Coch L, Berzigotti A, et al. Antiangiogenic and antifibrogenic activity of pigment epithelium-derived factor (PEDF) in bile duct-ligated portal hypertensive rats. Gut 2015;64:657–666.
17. Filleur S, Volz K, Nelius T, et al. Two functional epitopes of pigment epithelial-derived factor block angiogenesis and induce differentiation in prostate cancer. Cancer Res 2005;65:5144–5152.
18. Crawford SE, Stellmach V, Ranalli M, et al. Pigment epithelium-derived factor (PEDF) in neuroblastoma: a multifunctional mediator of Schwann cell antitumor activity. J Cell Sci 2001;114:4421–4428.
19. Park K, Lee K, Zhang B, et al. Identification of a novel inhibitor of the canonical Wnt pathway. Mol Cell Biol 2011;31:3038–3051.
20. Tombran-Tink J, Mazuruk K, Rodriguez IR, et al. Organization, evolutionary conservation, expression and unusual Alu density of the human gene for pigment epithelium-derived factor, a unique neurotrophic serpin. Mol Vis 1996;2:11.

21. Uhlen M, Fagerberg L, Hallstrom BM, et al. Proteomics. Tissue-based map of the human proteome. Science 2015;347:1260419.
22. Gattu AK, Swenson ES, Iwakiri Y, et al. Determination of mesenchymal stem cell fate by pigment epithelium-derived factor (PEDF) results in increased adiposity and reduced bone mineral content. Faseb J 2013; 27:4384–4394.
23. Subramanian A, Tamayo P, Mootha VK, et al. Gene set enrichment analysis: a knowledge-based approach for interpreting genome-wide expression profiles. Proc Natl Acad Sci U S A 2005;102:15545–15550.
24. Gattu AK, Birkenfeld AL, Iwakiri Y, et al. Pigment epithelium-derived factor (PEDF) suppresses IL-1beta-mediated c-Jun N-terminal kinase (JNK) activation to improve hepatocyte insulin signaling. Endocrinology 2014:en20131785.
25. Amaral J, Becerra SP. Effects of human recombinant PEDF protein and PEDF-derived peptide 34-mer on choroidal neovascularization. Invest Ophthalmol Vis Sci 2010;51:1318–1326.
26. Cox G, Kable E, Jones A, et al. 3-dimensional imaging of collagen using second harmonic generation. J Struct Biol 2003;141:53–62.
27. Torres R, Vesuna S, Levene MJ. High-resolution, 2- and 3-dimensional imaging of uncut, unembedded tissue biopsy samples. Arch Pathol Lab Med 2014; 138:395–402.
28. Mikels AJ, Nusse R. Purified Wnt5a protein activates or inhibits beta-catenin-TCF signaling depending on receptor context. PLoS Biol 2006;4:e115.
29. Cairo S, Armengol C, De Reynies A, et al. Hepatic stem-like phenotype and interplay of Wnt/beta-catenin and Myc signaling in aggressive childhood liver cancer. Cancer Cell 2008;14:471–484.
30. Chiang DY, Villanueva A, Hoshida Y, et al. Focal gains of VEGFA and molecular classification of hepatocellular carcinoma. Cancer Res 2008;68:6779–6788.
31. Cavard C, Terris B, Grimber G, et al. Overexpression of regenerating islet-derived 1 alpha and 3 alpha genes in human primary liver tumors with beta-catenin mutations. Oncogene 2006;25:599–608.
32. Kenny PA, Enver T, Ashworth A. Receptor and secreted targets of Wnt-1/beta-catenin signalling in mouse mammary epithelial cells. BMC Cancer 2005;5:3.
33. Merle P, de la Monte S, Kim M, et al. Functional consequences of frizzled-7 receptor overexpression in human hepatocellular carcinoma. Gastroenterology 2004;127:1110–1122.
34. Fernandez M, Semela D, Bruix J, et al. Angiogenesis in liver disease. J Hepatol 2009;50:604–620.
35. Nejak-Bowen KN, Monga SP. Beta-catenin signaling, liver regeneration and hepatocellular cancer: sorting the good from the bad. Semin Cancer Biol 2011;21:44–58.
36. Zhang XF, Tan X, Zeng G, et al. Conditional beta-catenin loss in mice promotes chemical hepatocarcinogenesis: role of oxidative stress and platelet-derived growth factor receptor alpha/phosphoinositide 3-kinase signaling. Hepatology 2010;52:954–965.
37. Brack AS, Conboy MJ, Roy S, et al. Increased Wnt signaling during aging alters muscle stem cell fate and increases fibrosis. Science 2007;317:807–810.
38. Cheng JH, She H, Han YP, et al. Wnt antagonism inhibits hepatic stellate cell activation and liver fibrosis. Am J Physiol Gastrointest Liver Physiol 2008;294:G39–49.
39. DiRocco DP, Kobayashi A, Taketo MM, et al. Wnt4/beta-catenin signaling in medullary kidney myofibroblasts. J Am Soc Nephrol 2013;24:1399–1412.
40. Becker J, Semler O, Gilissen C, et al. Exome sequencing identifies truncating mutations in human SERPINF1 in autosomal-recessive osteogenesis imperfecta. Am J Hum Genet 2011;88:362–371.
41. Li F, Song N, Tombran-Tink J, Niyibizi C. Pigment epithelium derived factor suppresses expression of Sost/sclerostin by osteocytes: implication for its role in bone matrix mineralization. J Cell Physiol 2015;230: 1243–1249.
42. Li F, Song N, Tombran-Tink J, Niyibizi C. Pigment epithelium-derived factor enhances differentiation and mineral deposition of human mesenchymal stem cells. Stem Cells 2013;31:2714–2723.
43. Cruciat CM, Niehrs C. Secreted and transmembrane wnt inhibitors and activators. Cold Spring Harb Perspect Biol 2013;5:a015081.
44. Brott BK, Sokol SY. Regulation of Wnt/LRP signaling by distinct domains of Dickkopf proteins. Mol Cell Biol 2002; 22:6100–6110.

Received November 26, 2014. Accepted June 2, 2015.

Correspondence
Address correspondence to: Chuhan Chung, MD, Section of Digestive Diseases, Department of Medicine, 1080 LMP, Yale University School of Medicine, New Haven, Connecticut 06519. e-mail: chuhan.chung@yale.edu.

Acknowledgements
The authors thank Kathy Harry (Yale Liver Center) and Edward J. Edmonds (VA Connecticut Healthcare) for expert technical assistance.

Conflicts of interest
The authors disclose no conflicts.

Funding
This study was funded by Digestive Diseases Research Core Centers–5P30DK034989 (to C.C.); Yale Core Center for Musculoskeletal Disorders P30-AR46032; Veterans Affairs Merit Grant (to C.C.).

Supplementary Table 1. List of Statistically Significant Differentially Expressed Gene Entities in PEDF Knockout Animals Versus Wild-Type (FDR < .05 and Expression Cutoff of 1.3-Fold)

Symbol	Fold Up	Symbol	Fold Down
Cyp2b9	6.730	Serpinf1 (KO GENE)	−143.796
Gsta1	4.853	Serpina1e	−8.049
Cyp2b23	4.285	Hsd3b5	−5.549
Ly6d	4.166	Lpin1	−3.815
Gsta2	3.822	Serpina4-ps1	−3.642
Tubb2b	3.390	Nnmt	−3.193
Lcn2	3.346	Nnmt	−3.105
Anxa2	2.943	Egfr	−3.080
Mod1	2.733	C6	−3.023
Cidec	2.654	Egfr	−2.957
S100a11	2.579	Aatk	−2.871
Bcl6	2.524	C8b	−2.749
Orm2	2.467	Egfr	−2.578
Wfdc2	2.254	C6	−2.577
Aqp8	2.222	Cyp7b1	−2.553
Insig2	2.192	Cyp4a12b	−2.465
Tceal8	2.169	Clca3	−2.437
Lgals3	2.167	Sds	−2.380
Spon2	2.165	Slc38a2	−2.378
Aqp8	2.127	Ela1	−2.333
Ubd	2.079	2200001I15Rik	−2.305
H2-Ab1	2.062	Cyp7a1	−2.302
Apoa4	2.056	Fbxo31	−2.246
Cbr3	2.053	EG13909	−2.223
Hsd17b6	1.980	Selenbp2	−2.181
Lpl	1.978	Socs2	−2.177
Cd74	1.972	Upp2	−2.167
Raet1b	1.967	Fbxo31	−2.165
Egr1	1.965	Tsc22d3	−2.161
Pdk4	1.927	C8a	−2.142
Ttc39a	1.900	Cyp4f14	−2.136
Slc17a4	1.878	2810439F02Rik	−2.120
Gstm2	1.850	Slc29a1	−2.110
Sqle	1.829	F11	−2.106
Spp1	1.793	Siat9	−2.095
Ccnd1	1.788	Mup4	−2.095
H2-Aa	1.786	LOC100047762	−2.070
Sepp1	1.785	Cish	−2.065
H2-Ab1	1.780	Ptpre	−2.059
Insig2	1.735	Por	−2.055
Cd74	1.734	Ccrn4l	−2.022
Insig2	1.734	Hpd	−2.013
Aqp4	1.724	Upp2	−1.984
Vldlr	1.724	Prei4	−1.980
Srxn1	1.722	F11	−1.978
Elovl6	1.711	Prodh	−1.961
Slpi	1.707	Zap70	−1.960

Supplementary Table 1. Continued

Symbol	Fold Up	Symbol	Fold Down
Lgals1	1.706	Por	−1.960
Gdf15	1.696	Zxda	−1.954
Ptp4a2	1.690	Gne	−1.950
LOC100047046	1.689	Kcnk5	−1.918
LOC641240	1.684	Pptc7	−1.906
Limk1	1.683	Eif4ebp3	−1.894
Ntrk2	1.680	2810439F02Rik	−1.890
H2-Ab1	1.679	Tk1	−1.879
Gstm2	1.679	Zap70	−1.875
Fam129b	1.676	Tef	−1.871
Col6a1	1.673	Angptl4	−1.851
Ctps	1.672	Chac1	−1.838
Nudt18	1.669	Gm129	−1.836
Anxa5	1.668	Agxt	−1.835
Zfp36l1	1.664	Lpin2	−1.835
Ankrd56	1.658	EG13909	−1.834
H2-Eb1	1.652	Asl	−1.824
S100a10	1.648	Afmid	−1.821
Ccnd1	1.642	Tle1	−1.820
Srxn1	1.641	Afmid	−1.820
Lyzs	1.639	Spata2L	−1.817
Cd63	1.637	Upp2	−1.814
Idh2	1.634	St3gal5	−1.802
Uhrf1	1.633	Chka	−1.802
Uap1l1	1.632	rp9	−1.797
Dusp6	1.625	Smarcd2	−1.796
Aldh1a1	1.623	Gpt1	−1.792
Mfge8	1.619	Cyp4f13	−1.784
Acnat2	1.614	Nrbp2	−1.784
Cxcl9	1.614	Cps1	−1.778
Acly	1.609	Cebpb	−1.773
Tsc22d1	1.609	Serpinf2	−1.762
Rtn4rl1	1.597	Hs6st1	−1.757
Plekha1	1.596	Gls2	−1.750
Cyp4a14	1.595	Susd4	−1.750
Usp18	1.594	Apom	−1.744
Cd9	1.591	Klhl21	−1.744
Smpd3	1.591	Fkbp5	−1.743
Hist1h2ao	1.590	Prhoxnb	−1.743
Col4a1	1.587	Cbs	−1.741
Lypla1	1.583	Lgals4	−1.732
Gstm2	1.583	Ccbl1	−1.727
Rcan1	1.582	Upp2	−1.726
Tlr2	1.571	Foxa3	−1.724
Prune	1.569	Sardh	−1.711
LOC100043671	1.567	Clec2d	−1.710
Lgals3bp	1.567	B230342M21Rik	−1.708
Ccbl2	1.567	Afmid	−1.708
Hrsp12	1.566	Bach1	−1.708
Elovl5	1.562	Tmem50a	−1.707

Supplementary Table 1. Continued

Symbol	Fold Up	Symbol	Fold Down
Ccnd1	1.560	Mlxipl	−1.706
Gadd45a	1.559	Gcgr	−1.703
Samd9l	1.556	Agpat6	−1.697
Gas6	1.555	Cyp4f15	−1.693
Esd	1.549	Plg	−1.692
Cyp3a11	1.548	Cyp1a2	−1.687
Sparc	1.547	Serpina3k	−1.676
LOC100047934	1.542	D4Bwg0951e	−1.675
Ctsa	1.538	Nfic	−1.673
Ppic	1.536	Hhex	−1.671
Nipsnap3a	1.536	Ush2a	−1.670
Mcm6	1.533	Ang	−1.668
Axl	1.531	Hyal1	−1.666
Tmem43	1.530	Pgls	−1.663
Plscr1	1.528	Itih3	−1.662
Lum	1.526	Rnase4	−1.659
2410004L22Rik	1.526	Ttc36	−1.655
Cdkn1a	1.523	1700019G17Rik	−1.651
Arl8a	1.521	Cps1	−1.650
Acot4	1.519	Rps5	−1.646
Laptm5	1.515	9530058B02Rik	−1.643
St5	1.515	2310076L09Rik	−1.642
Gbp2	1.515	Il6ra	−1.638
Sirpa	1.513	Mbd1	−1.638
Ifi27	1.512	Atp5sl	−1.635
Sqle	1.511	Kcnk5	−1.635
Acot3	1.509	Gnat1	−1.634
Spc25	1.505	Abcg8	−1.629
B930041F14Rik	1.504	Tmem160	−1.622
Tgfbr2	1.502	Hist1h2bm	−1.621
Tgm2	1.502	Hes6	−1.619
Cbr3	1.500	Asl	−1.618
Aldh1a7	1.500	Acaa2	−1.617
Hprt1	1.497	Zfp259	−1.617
Entpd5	1.497	Klf13	−1.612
Cyba	1.497	Hist2h2aa1	−1.607
Tpm1	1.496	Ccbl1	−1.593
Acox1	1.495	Npr2	−1.593
Cyp4a31	1.493	Map1lc3a	−1.592
Atp5a1	1.492	Ephx2	−1.590
Col6a1	1.489	Tmem183a	−1.587
Dusp6	1.488	Scnn1a	−1.586
Tmem77	1.486	Afmid	−1.586
Fos	1.483	Igfals	−1.582
LOC100048346	1.483	Fgf1	−1.582
Ifit3	1.482	Cnpy2	−1.582
Ctsc	1.480	0610012D14Rik	−1.582
Serpina7	1.480	Tspan31	−1.581
Pex11a	1.478	Rbm5	−1.580
Ccdc80	1.475	Ugt2b1	−1.580

Supplementary Table 1. Continued

Symbol	Fold Up	Symbol	Fold Down
Rnf125	1.475	Med25	−1.578
Tm4sf4	1.475	Eif4ebp1	−1.578
St5	1.474	Serpina11	−1.577
Col5a1	1.474	Ass1	−1.577
Cyp2a5	1.474	Nfkbia	−1.574
Enc1	1.473	Lcat	−1.573
Plscr1	1.472	Rps10	−1.572
Aldh1b1	1.470	Atad3a	−1.571
Lamb3	1.469	Hist1h2bn	−1.570
Cdc20	1.468	Upb1	−1.568
Cxcl10	1.468	Cpsf4l	−1.563
H2-DMb1	1.467	Fn3k	−1.563
Vps29	1.466	Klf9	−1.561
Igf2bp2	1.466	Ivd	−1.558
Csf1r	1.464	Prodh2	−1.558
Ear2	1.463	Mcm10	−1.558
Cyp2c29	1.460	Mrpl55	−1.557
Dsp	1.460	Prodh2	−1.556
Tubb6	1.459	Sri	−1.555
Ctsc	1.459	Eef2	−1.552
Tnfrsf22	1.458	Pla1a	−1.551
Gadd45a	1.458	Cisd1	−1.551
Mmp2	1.453	Serpinf2	−1.549
Gstm1	1.451	P2ry1	−1.547
Cd52	1.448	4933426M11Rik	−1.547
Vldlr	1.445	Alas1	−1.546
Aadac	1.444	Dedd2	−1.540
Glul	1.444	Pipox	−1.536
Bcap31	1.443	Fam152b	−1.535
Ly6a	1.442	1300017J02Rik	−1.530
Abcb11	1.441	Abcc6	−1.529
Loxl1	1.441	Sema4g	−1.529
Col4a2	1.436	BC031353	−1.529
Mvd	1.436	Brap	−1.528
Il1b	1.434	Lsm4	−1.527
Mcm4	1.433	Slc38a3	−1.527
Slc13a3	1.432	Pex6	−1.526
Net1	1.432	Nfix	−1.521
Hist1h2ak	1.430	Als2	−1.520
Ugt2b35	1.430	Errfi1	−1.519
Apoc2	1.428	Ldb1	−1.518
Mcm5	1.426	Hc	−1.516
Rnd2	1.426	Ptms	−1.516
Gclc	1.426	Agt	−1.516
Pparg	1.425	Igf1	−1.515
Gpam	1.425	Akr7a5	−1.515
Osbpl3	1.425	Ddx6	−1.513
Slc41a2	1.422	Hpn	−1.513
Tnfaip2	1.422	Stard10	−1.513
Tmsb4x	1.421	Mafg	−1.511

Supplementary Table 1. Continued

Symbol	Fold Up	Symbol	Fold Down
Mcm6	1.420	Tsku	−1.510
Khk	1.417	Cyp2c37	−1.508
Fam110a	1.416	Rpl34	−1.508
Mme	1.416	Rbm4b	−1.507
LOC677317	1.415	Bmp1	−1.506
4931406C07Rik	1.414	Wdr45l	−1.506
Klf6	1.412	Afmid	−1.505
Ywhah	1.411	Ppp1r10	−1.505
LOC100047963	1.409	Afmid	−1.504
Nampt	1.409	Pop5	−1.504
Hist1h2af	1.408	4833421E05Rik	−1.502
Emr1	1.406	OTTMUSG00000000231	−1.502
Dapk2	1.405	Pscd1	−1.500
S100a8	1.404	Vgll4	−1.499
Hprt1	1.403	F7	−1.499
1810023F06Rik	1.401	Tmem42	−1.499
Ndufa5	1.401	Gm129	−1.497
Bmp4	1.399	Saps3	−1.496
Akr1c14	1.397	Cyp2c67	−1.496
Cyp2c39	1.395	Oat	−1.495
Vldlr	1.395	1110001J03Rik	−1.494
Nqo1	1.394	Glyctk	−1.494
Jun	1.394	Srrm2	−1.492
LOC100048733	1.394	Tst	−1.492
Tm4sf4	1.393	Sdsl	−1.492
Rtn4	1.391	Fgg	−1.491
Iqgap1	1.391	Hist1h2bk	−1.490
Arhgdib	1.391	Klf1	−1.490
Rcan2	1.389	F2	−1.490
Palmd	1.388	Elovl3	−1.487
Hist1h2an	1.387	Ctdsp2	−1.485
Rcan2	1.386	Cbs	−1.485
Tmem49	1.385	Ppm1k	−1.483
Entpd5	1.384	Cyp1a2	−1.483
Idi1	1.382	Hsp105	−1.482
Nsdhl	1.381	1110032A13Rik	−1.481
Slamf9	1.381	H2afy	−1.480
Trim2	1.380	Dnajb6	−1.480
Lip1	1.377	Keg1	−1.480
6330409N04Rik	1.376	Slc35b2	−1.480
9030625A04Rik	1.376	Tmem19	−1.479
Cxadr	1.376	Fam125a	−1.478
Pltp	1.375	Gde1	−1.478
Agpat9	1.375	Gpr182	−1.477
Zfp608	1.375	D9Wsu20e	−1.477
Gale	1.375	Gpr108	−1.475
Rasl11b	1.374	Rps8	−1.475
Tpm4	1.374	Lman1	−1.475
Saa2	1.374	Rpl23	−1.474
BC005537	1.372	Zfp91-cntf	−1.474

Supplementary Table 1. Continued

Symbol	Fold Up	Symbol	Fold Down
Mcm2	1.372	Upf1	−1.473
Lhfp	1.370	F10	−1.473
Slc23a2	1.369	Acot1	−1.472
Usp18	1.368	Slc1a2	−1.472
Ppp1r3c	1.367	Prodh2	−1.468
Cpxm1	1.366	Ap3m1	−1.468
LOC100046254	1.365	Fbxo33	−1.467
Junb	1.364	Slc25a42	−1.467
2010311D03Rik	1.363	Qdpr	−1.466
Krt8	1.363	Hbs1l	−1.466
Angptl3	1.360	Pcsk4	−1.465
Orm1	1.360	Tut1	−1.465
Emp1	1.359	Sec14l4	−1.465
Gca	1.359	Slc7a2	−1.464
Nid1	1.358	Gstp1	−1.464
Ddx3x	1.357	Glt25d1	−1.464
Ebpl	1.354	Tmem160	−1.464
Slc13a3	1.353	Smarca2	−1.464
Btg1	1.353	Pxmp2	−1.463
Tnip1	1.352	Zfp276	−1.463
Tmem43	1.352	Nosip	−1.463
Pparg	1.352	Cml1	−1.463
Serinc2	1.351	Tmprss6	−1.462
Col15a1	1.350	Scara5	−1.462
LOC433801	1.350	Mup5	−1.460
Cyp3a25	1.349	Cadps2	−1.459
Gale	1.347	Rsn	−1.459
Id2	1.347	EG665378	−1.458
LOC668837	1.346	Pop5	−1.458
Slc6a8	1.345	Igfbp4	−1.456
Vim	1.345	Mbl1	−1.455
Cd274	1.345	Rps25	−1.455
Mfge8	1.342	Crcp	−1.455
Tnfrsf19	1.342	Plxna1	−1.454
Rnf125	1.341	Zfp771	−1.454
Mlkl	1.341	Serpina1a	−1.454
EG277333	1.340	Trfr2	−1.453
Adam9	1.339	Foxo1	−1.453
Pgrmc1	1.338	Dnajc3	−1.452
Mat2a	1.337	LOC622404	−1.452
Ccbl2	1.336	Sec63	−1.451
Tnfaip2	1.336	Tmem150	−1.451
Pip4k2a	1.335	Sepx1	−1.451
Mad2l1	1.335	Slc6a12	−1.451
Adra2b	1.334	Hist1h2bj	−1.451
Snx7	1.333	Xpa	−1.449
Chmp5	1.332	Syt1	−1.448
Gsta4	1.331	Trap1	−1.447
Pigp	1.330	Tnrc6a	−1.446
Mreg	1.329	Ercc5	−1.446

Supplementary Table 1. Continued

Symbol	Fold Up	Symbol	Fold Down
Rnd3	1.329	Sil1	−1.445
Nit2	1.328	9430029K10Rik	−1.445
Cxadr	1.328	Gltpd2	−1.445
Cotl1	1.323	Cxxc1	−1.444
2900064A13Rik	1.323	Trp53inp2	−1.443
Lrrc39	1.323	Serinc3	−1.443
Dld	1.322	Trak1	−1.443
Pmpcb	1.321	Arfgap2	−1.443
Rab34	1.320	Iyd	−1.442
Fas	1.320	Tnrc6c	−1.442
Hist1h2ah	1.320	Hint2	−1.442
Fen1	1.320	0610012G03Rik	−1.442
Hsd17b11	1.320	Coq5	−1.441
Tnxb	1.319	Gls2	−1.441
Saa1	1.319	Rpain	−1.439
Tnfrsf12a	1.317	Surf1	−1.438
Acot2	1.317	Ube3b	−1.437
Cd53	1.317	Mrps21	−1.437
Entpd2	1.316	Eif4g1	−1.436
Ermp1	1.315	Hamp	−1.435
Cd86	1.315	Os9	−1.435
Tapbp	1.315	Ganab	−1.434
Cyp2c55	1.315	Mcm10	−1.432
2610305D13Rik	1.314	Rab43	−1.432
Ccl4	1.314	Rshl2a	−1.431
1700047I17Rik1	1.314	Spg20	−1.431
Snx3	1.313	Josd2	−1.430
Mcm6	1.312	Cyp2c70	−1.430
Ccdc120	1.310	Aldh16a1	−1.428
Slc16a6	1.310	Vkorc1	−1.428
Nipa1	1.308	Gorasp1	−1.428
Arl2bp	1.308	Dap	−1.427
1190002N15Rik	1.308	Pim3	−1.426
Cryl1	1.308	Aox3	−1.425
Litaf	1.307	Rps15	−1.425
Jak1	1.306	Cyp27a1	−1.425
Cdkn2c	1.306	2310007F21Rik	−1.425
Rhod	1.306	Acy1	−1.424
Bcl2l13	1.306	Mug2	−1.424
Acot10	1.305	Stk11	−1.424
Aifm1	1.303	Yif1b	−1.424
Phca	1.303	Irf3	−1.423
Arcn1	1.303	Fbxl10	−1.423
Esr1	1.303	Rapgef4	−1.423
Palld	1.301	Tm2d2	−1.422
Ldlr	1.301	Serpinf2	−1.422
Rab8b	1.300	Ceacam1	−1.422
		Csnk1g2	−1.422
		Hnrpc	−1.421
		Gpld1	−1.421

Supplementary Table 1. Continued

Symbol	Fold Up	Symbol	Fold Down
		Hist1h2bh	−1.421
		Ssr4	−1.421
		Bst2	−1.421
		Acox2	−1.421
		Sra1	−1.420
		Cyp2c37	−1.420
		Eif4ebp2	−1.420
		Atp13a1	−1.420
		Abat	−1.420
		Per2	−1.419
		Polr2f	−1.419
		Slc1a2	−1.419
		Bckdhb	−1.418
		Itih1	−1.418
		Pbld	−1.418
		Fam134a	−1.417
		Lgals4	−1.416
		LOC100047856	−1.416
		LOC100044324	−1.416
		2900010M23Rik	−1.415
		Rnase4	−1.415
		Vtn	−1.415
		Mrpl17	−1.414
		Stat3	−1.414
		Ankzf1	−1.414
		5133401N09Rik	−1.414
		Prpf8	−1.414
		Bckdha	−1.413
		Sirt7	−1.413
		C1rl	−1.413
		Ndufb10	−1.413
		EG13909	−1.413
		Mug4	−1.412
		Gnmt	−1.412
		Bloc1s1	−1.411
		Cuta	−1.411
		Vrk3	−1.411
		Fetub	−1.410
		Lims2	−1.409
		Tm7sf2	−1.407
		Gltpd2	−1.407
		Ppap2b	−1.407
		Prei4	−1.407
		Arl3	−1.407
		A430005L14Rik	−1.406
		Rpl36a	−1.406
		Dnajc7	−1.406
		Map2k2	−1.405
		Dym	−1.405
		Wdr45l	−1.404

Supplementary Table 1. Continued

Symbol	Fold Up	Symbol	Fold Down
		Plekhg3	−1.404
		Rps21	−1.404
		Ghr	−1.403
		Bmp1	−1.403
		Tle1	−1.403
		Ppargc1b	−1.402
		Acad10	−1.402
		Rpl12	−1.402
		Pnpo	−1.401
		Ddx3y	−1.401
		Galt	−1.401
		Smoc1	−1.401
		Cyp27a1	−1.399
		Clmn	−1.399
		3110056O03Rik	−1.399
		Tex264	−1.399
		Nat6	−1.398
		Pla2g12a	−1.397
		Srm	−1.396
		LOC100048020	−1.396
		Bat3	−1.396
		Tsc22d3	−1.396
		Mupcdh	−1.396
		Acat1	−1.396
		Cib1	−1.396
		Exosc5	−1.396
		1300007L22Rik	−1.396
		Sort1	−1.394
		LOC545056	−1.394
		Gtf3c1	−1.392
		Myo18a	−1.392
		LOC100048105	−1.392
		Csnk2a2	−1.391
		Csnk1g3	−1.391
		Serpinc1	−1.391
		Mrps28	−1.391
		Aamp	−1.391
		Tha1	−1.391
		Aars	−1.390
		Cope	−1.390
		Bri3	−1.390
		Nme3	−1.389
		Ppp1r3b	−1.389
		Ccdc84	−1.389
		Sirt3	−1.388
		1500032D16Rik	−1.388
		Mrps26	−1.388
		Ict1	−1.387
		Tpst1	−1.387
		Prpf38b	−1.387

Supplementary Table 1. Continued

Symbol	Fold Up	Symbol	Fold Down
		Als2	−1.387
		Klkb1	−1.387
		MGC18837	−1.386
		Dcxr	−1.386
		1700029P11Rik	−1.386
		Gaa	−1.385
		1700012H05Rik	−1.385
		Gnl3	−1.385
		Hdgf	−1.385
		Aifm1	−1.385
		Tcf25	−1.384
		Sdc2	−1.384
		Mtss1	−1.384
		Atf2	−1.384
		Cyp2c67	−1.383
		Eef2	−1.383
		Mrpl2	−1.383
		Usp2	−1.382
		Timm10	−1.382
		Fkbp8	−1.382
		0610012D14Rik	−1.382
		3300001P08Rik	−1.382
		F12	−1.381
		2010100O12Rik	−1.381
		Slc26a1	−1.381
		Paox	−1.380
		Afmid	−1.380
		Dpp3	−1.380
		Dpm2	−1.379
		St3gal3	−1.378
		Serpina1a	−1.378
		2810428I15Rik	−1.377
		Akr7a5	−1.377
		6430527G18Rik	−1.377
		D19Wsu162e	−1.376
		Phb2	−1.376
		Trabd	−1.376
		Txnl4a	−1.376
		Macrod1	−1.376
		Gamt	−1.375
		Lgsn	−1.374
		Atp5g2	−1.374
		Jmjd6	−1.373
		Cyp27a1	−1.373
		Cno	−1.373
		Naprt1	−1.372
		Hpn	−1.372
		Il1rap	−1.371
		Rnf6	−1.370
		Atp1a1	−1.370

Supplementary Table 1. Continued

Symbol	Fold Up	Symbol	Fold Down
		Yeats4	−1.370
		Lmf1	−1.370
		Bcas3	−1.370
		Echdc2	−1.370
		Acot12	−1.370
		Kng1	−1.369
		Hsd17b10	−1.369
		Upb1	−1.369
		D17Wsu92e	−1.369
		Taf10	−1.369
		Keap1	−1.368
		Pdcd5	−1.368
		Plekhb1	−1.368
		Mthfd1	−1.368
		Nr1h4	−1.367
		BC031181	−1.366
		Fpgs	−1.366
		Gphn	−1.366
		Ccar1	−1.366
		Stard5	−1.366
		Slc25a38	−1.365
		Ccdc21	−1.365
		Psmc5	−1.364
		C130074G19Rik	−1.364
		0610007P22Rik	−1.364
		Dalrd3	−1.364
		Mib2	−1.363
		Tsc2	−1.363
		Sec63	−1.363
		Myo6	−1.362
		Abtb1	−1.362
		1110008F13Rik	−1.362
		Tspan33	−1.362
		Mettl7b	−1.361
		LOC100048445	−1.361
		BC021381	−1.361
		H13	−1.361
		Zfp91	−1.361
		Arfl4	−1.360
		1810008A18Rik	−1.359
		Tlcd2	−1.359
		Ube2l3	−1.359
		6430706D22Rik	−1.359
		Prpf6	−1.359
		Cebpa	−1.358
		Tsta3	−1.358
		Aspscr1	−1.358
		Gphn	−1.357
		Ccnt1	−1.357
		Prox1	−1.357

Supplementary Table 1. Continued

Symbol	Fold Up	Symbol	Fold Down
		Dph2	−1.356
		Nr1h2	−1.356
		Dcxr	−1.355
		Arg1	−1.355
		Per1	−1.355
		Cox4i1	−1.355
		1700021F05Rik	−1.354
		Masp2	−1.354
		9530058B02Rik	−1.354
		Sf3b5	−1.353
		Ctdsp1	−1.353
		Akap8l	−1.352
		Slc37a4	−1.351
		Rab18	−1.351
		Mrps34	−1.351
		Mfsd2	−1.350
		Ext2	−1.350
		Ttyh2	−1.350
		Dnajb2	−1.350
		Lsm12	−1.349
		Ddx24	−1.349
		Tmem201	−1.349
		Fh1	−1.348
		Cpn1	−1.348
		Cxxc1	−1.348
		Isy1	−1.347
		Srm	−1.347
		Ythdf1	−1.347
		Derl2	−1.346
		Csrp2	−1.346
		Gnmt	−1.346
		Mfn1	−1.346
		Igfbp4	−1.345
		Rnf166	−1.345
		LOC100048105	−1.345
		2700038C09Rik	−1.345
		Herpud1	−1.345
		Trfr2	−1.344
		BC056474	−1.343
		Mon1a	−1.343
		Itih4	−1.343
		Upf1	−1.342
		Rpl19	−1.342
		Gdi1	−1.342
		Echdc2	−1.341
		5730453I16Rik	−1.340
		Eif3g	−1.340
		Dgcr2	−1.340
		Fbxo34	−1.340
		Mett11d1	−1.340

Supplementary Table 1. Continued

Symbol	Fold Up	Symbol	Fold Down
		Ngef	−1.340
		Fastk	−1.340
		Pex6	−1.340
		Dexi	−1.340
		Bclaf1	−1.339
		Use1	−1.339
		Zfp607	−1.338
		EG545056	−1.338
		Ugt2a3	−1.338
		Uspl1	−1.337
		Cope	−1.337
		Arrdc2	−1.337
		C1rl	−1.336
		Rabac1	−1.336
		Anp32a	−1.336
		Rilp	−1.336
		Prr14	−1.336
		620807	−1.336
		Limd1	−1.335
		Ctsf	−1.335
		Lemd2	−1.335
		Lamp2	−1.335
		Cldn3	−1.335
		Nol5	−1.335
		Man2c1	−1.334
		Scarb2	−1.333
		Igf1	−1.333
		S100a13	−1.333
		LOC100047937	−1.333
		Zbtb7a	−1.332
		Ogfod2	−1.332
		B3gnt1	−1.332
		Zbtb22	−1.331
		Atp6v0a1	−1.331
		Pnpla2	−1.331
		Plg	−1.331
		Sdhb	−1.330
		Cdo1	−1.329
		Ilvbl	−1.329
		6720456B07Rik	−1.329
		Map1lc3b	−1.329
		Smarca2	−1.328
		Fars2	−1.328
		Whdc1	−1.328
		1110032A13Rik	−1.327
		Dmwd	−1.327
		Morc3	−1.327
		Myg1	−1.327
		Scap	−1.327
		Itfg3	−1.327

Supplementary Table 1. Continued

Symbol	Fold Up	Symbol	Fold Down
		1110007A13Rik	−1.326
		Cmtm8	−1.326
		Wipi2	−1.326
		1110007L15Rik	−1.326
		Vkorc1	−1.326
		Eif3eip	−1.325
		1810020D17Rik	−1.325
		Dexi	−1.325
		Rpl28	−1.325
		Slc6a9	−1.324
		Jmjd3	−1.324
		1300001I01Rik	−1.324
		Cog8	−1.324
		Irf3	−1.324
		Chmp2a	−1.324
		D19Bwg1357e	−1.323
		Itpr2	−1.323
		LOC100047935	−1.323
		H2-Ke6	−1.323
		Mrpl3	−1.322
		Mrpl34	−1.322
		Slc25a39	−1.322
		Spcs3	−1.321
		Dhrs4	−1.321
		Ppp1r9a	−1.321
		Nags	−1.321
		Keap1	−1.321
		Cox7a2l	−1.320
		Mocs1	−1.320
		Sap30l	−1.320
		C630028N24Rik	−1.319
		Zfand2b	−1.319
		LOC100045697	−1.319
		Pdcd2	−1.318
		Yipf3	−1.318
		Ctdsp1	−1.318
		Mrps9	−1.318
		Plg	−1.317
		Upb1	−1.317
		B020018G12Rik	−1.317
		Il1rap	−1.317
		Gchfr	−1.316
		Rab3gap1	−1.316
		Slc35e3	−1.316
		Rufy3	−1.316
		Tmem63b	−1.316
		Ndufv2	−1.316
		Pde4dip	−1.315
		Avpr1a	−1.315
		Ogfr	−1.315

Supplementary Table 1. Continued

Symbol	Fold Up	Symbol	Fold Down
		Tec	−1.314
		Golga2	−1.314
		Acads	−1.314
		Tnrc6a	−1.314
		Sbf1	−1.314
		Faah	−1.314
		1810026J23Rik	−1.314
		Arl3	−1.313
		Tmem14c	−1.313
		Brms1	−1.313
		Qprt	−1.313
		Atp5d	−1.312
		Slc2a9	−1.312
		Sdc4	−1.312
		Eif1b	−1.311
		Prdx4	−1.311
		Dmtf1	−1.311
		Il6st	−1.311
		Tmem204	−1.311
		Rnaseh2c	−1.311
		Aldh1l1	−1.310
		Fis1	−1.310
		Clcn2	−1.310
		Impdh2	−1.310
		Cdk8	−1.309
		Wdr45	−1.309
		Creb3l3	−1.308
		Aes	−1.308
		Riok3	−1.308
		Mta2	−1.308
		Slc12a2	−1.308
		Morf4l1	−1.307
		Trpc4ap	−1.307
		Tmem53	−1.307
		2310044H10Rik	−1.307
		Snrpd2	−1.307
		Cxcl12	−1.306
		Lcat	−1.306
		Depdc6	−1.306
		Imp3	−1.306
		2610003J06Rik	−1.306
		Proc	−1.306
		Fbxo34	−1.305
		Dbp	−1.305
		Etfb	−1.305
		Mrpl27	−1.305
		Bola2	−1.305
		Elof1	−1.305
		Cmtm8	−1.305
		Enpp1	−1.305

Supplementary Table 1. Continued

Symbol	Fold Up	Symbol	Fold Down
		2410015M20Rik	−1.304
		Polr1a	−1.304
		Pih1d1	−1.304
		Xrcc6	−1.304
		Mbl2	−1.304
		Naca	−1.304
		F12	−1.304
		2310003H01Rik	−1.303
		Fxyd1	−1.303
		Tacc1	−1.303
		Gemin4	−1.303
		Slc1a2	−1.303
		Txn2	−1.302
		Gpt2	−1.302
		LOC100045782	−1.302
		Slc9a3r1	−1.302
		Elavl1	−1.302
		AA415398	−1.301
		Sox5	−1.301
		Tmem143	−1.300
		Rab8a	−1.300
		Atg2a	−1.300

Supplementary Table 2. Full List of Significantly Enriched Canonical Pathways and Gene Ontology Categories Modulated in PEDF Knockout Mice Livers

Up-Regulated Canonical Pathways [DATABASE_PATHWAY NAME]

Database Web Link: (http://www.broadinstitute.org/gsea/msigdb/genesets.jsp?collection=CP)

Name	NES	FDR q Value
KEGG_GLUTATHIONE_METABOLISM	2.329	<.001
PID_INTEGRIN1_PATHWAY	2.221	.003
REACTOME_COLLAGEN_FORMATION	2.168	.006
REACTOME_GLUTATHIONE_CONJUGATION	2.136	.008
REACTOME_NCAM1_INTERACTIONS	2.089	.013
PID_SYNDECAN_1_PATHWAY	2.080	.013
PID_FOXM1PATHWAY	2.099	.014
REACTOME_EXTRACELLULAR_MATRIX_ORGANIZATION	2.057	.016
KEGG_METABOLISM_OF_XENOBIOTICS_BY_CYTOCHROME_P450	2.010	.020
KEGG_ECM_RECEPTOR_INTERACTION	2.029	.021
KEGG_HEMATOPOIETIC_CELL_LINEAGE	2.013	.022
PID_AVB3_INTEGRIN_PATHWAY	1.986	.024
PID_NFAT_TFPATHWAY	1.979	.024
REACTOME_INTERFERON_ALPHA_BETA_SIGNALING	1.966	.024
KEGG_DRUG_METABOLISM_CYTOCHROME_P450	1.971	.025
KEGG_CELL_CYCLE	1.915	.032
KEGG_DNA_REPLICATION	1.918	.033
REACTOME_DNA_STRAND_ELONGATION	1.923	.033
PID_TOLL_ENDOGENOUS_PATHWAY	1.928	.034
PID_FRA_PATHWAY	1.879	.046
KEGG_CYTOKINE_CYTOKINE_RECEPTOR_INTERACTION	1.864	.049

Down-Regulated Canonical Pathways [DATABASE_PATHWAY NAME]

Database Web Link: (http://www.broadinstitute.org/gsea/msigdb/genesets.jsp?collection=CP)

Name	NES	FDR *q* Value
REACTOME_PEPTIDE_CHAIN_ELONGATION	−2.878	<.001
REACTOME_TRANSLATION	−2.873	<.001
REACTOME_INFLUENZA_VIRAL_RNA_TRANSCRIPTION_AND_REPLICATION	−2.840	<.001
REACTOME_3_UTR_MEDIATED_TRANSLATIONAL_REGULATION	−2.827	<.001
KEGG_RIBOSOME	−2.821	<.001
REACTOME_NONSENSE_MEDIATED_DECAY_ENHANCED_BY_THE_EXON_JUNCT_COMPLEX	−2.797	<.001
REACTOME_SRP_DEPENDENT_COTRANSLATIONAL_PROTEIN_TARGETING_TO_MEMBRANE	−2.718	<.001
REACTOME_INFLUENZA_LIFE_CYCLE	−2.571	<.001
REACTOME_METABOLISM_OF_MRNA	−2.565	<.001
REACTOME_METABOLISM_OF_AMINO_ACIDS_AND_DERIVATIVES	−2.433	.005
REACTOME_METABOLISM_OF_RNA	−2.434	.005
REACTOME_ACTIVATION_OF_THE_MRNA_UPON_BINDING_OF_THE_CAP_BINDING_COMPLEX	−2.416	.005
REACTOME_FORMATION_OF_THE_TERNARY_COMPLEX	−2.419	.005
KEGG_GLYCINE_SERINE_AND_THREONINE_METABOLISM	−2.232	.049

Supplementary Table 2. Continued

Up-Regulated Gene Ontology Categories

Database Web Link: (http://www.broadinstitute.org/gsea/msigdb/genesets.jsp?collection=C5)

Name	NES	FDR *q* Value
GLUTATHIONE_TRANSFERASE_ACTIVITY	2.041	.039
COLLAGEN	2.049	.071
CYTOKINE_ACTIVITY	1.907	.109

Down-Regulated Gene Ontology Categories

Database Web Link: (http://www.broadinstitute.org/gsea/msigdb/genesets.jsp?collection=C5)

Name	NES	FDR *q* Value
STRUCTURAL_CONSTITUENT_OF_RIBOSOME	−2.790	<.001
MITOCHONDRIAL_PART	−2.287	.048
AMINO_ACID_AND_DERIVATIVE_METABOLIC_PROCESS	−2.185	.050
MITOCHONDRIAL_MATRIX	−2.173	.051
PROTEASE_INHIBITOR_ACTIVITY	−2.162	.051
CARBOXYLIC_ACID_METABOLIC_PROCESS	−2.244	.052
REGULATION_OF_ANGIOGENESIS	−2.198	.053
NITROGEN_COMPOUND_CATABOLIC_PROCESS	−2.186	.053
MITOCHONDRION	−2.292	.054
NITROGEN_COMPOUND_METABOLIC_PROCESS	−2.215	.054
MITOCHONDRIAL_LUMEN	−2.200	.056
SERINE_TYPE_ENDOPEPTIDASE_INHIBITOR_ACTIVITY	−2.224	.056
ANATOMICAL_STRUCTURE_FORMATION	−2.248	.056
MITOCHONDRIAL_ENVELOPE	−2.023	.057
ORGANELLE_INNER_MEMBRANE	−2.026	.059
AMINO_ACID_CATABOLIC_PROCESS	−2.005	.059
RIBOSOME	−2.031	.060
MITOCHONDRIAL_RIBOSOME	−2.047	.060
RIBOSOMAL_SUBUNIT	−2.250	.062
SPLICEOSOME	−1.977	.062
DNA_DIRECTED_RNA_POLYMERASEII_HOLOENZYME	−1.939	.062
MITOCHONDRIAL_MEMBRANE	−2.048	.063

Note: FDR (false-discovery rate), FDR *q* value; NES, normalized enrichment score.

Supplementary Table 3. Full List of Chemical and Genetic Perturbations That Were Significantly Enriched in PEDF KO Mice Livers

Up-Regulated Chemical and Genetic Perturbation Datasets
Up-Regulated List Truncated at FDR < .005

Database Web Link: (http://www.broadinstitute.org/gsea/msigdb/genesets.jsp?collection=CGP)

Name	NES	FDR *q* Value
LEE_LIVER_CANCER_ACOX1_UP	3.117	.000
LEE_LIVER_CANCER_E2F1_UP	3.017	.000
LEE_LIVER_CANCER_MYC_E2F1_UP	2.984	.000
LEE_LIVER_CANCER_MYC_TGFA_UP	2.911	.000
ICHIBA_GRAFT_VERSUS_HOST_DISEASE_35D_UP	2.892	.000
KHETCHOUMIAN_TRIM24_TARGETS_UP	2.891	.000
LEE_LIVER_CANCER_CIPROFIBRATE_UP	2.858	.000
LEE_LIVER_CANCER_DENA_UP	2.780	.000
WIELAND_UP_BY_HBV_INFECTION	2.772	.000
BORLAK_LIVER_CANCER_EGF_UP	2.742	.000
SERVITJA_LIVER_HNF1A_TARGETS_UP	2.742	.000
SHETH_LIVER_CANCER_VS_TXNIP_LOSS_PAM3	2.697	.000
SHETH_LIVER_CANCER_VS_TXNIP_LOSS_PAM2	2.635	.000
HESS_TARGETS_OF_HOXA9_AND_MEIS1_DN	2.622	.000
DEMAGALHAES_AGING_UP	2.605	.000
POOLA_INVASIVE_BREAST_CANCER_UP	2.580	.000
HECKER_IFNB1_TARGETS	2.516	.000
BOYAULT_LIVER_CANCER_SUBCLASS_G5_DN	2.507	.000
MCLACHLAN_DENTAL_CARIES_DN	2.476	.000
LE_EGR2_TARGETS_UP	2.445	.000
HOSHIDA_LIVER_CANCER_SUBCLASS_S1	2.403	.000
KIM_GLIS2_TARGETS_UP	2.390	.000
ICHIBA_GRAFT_VERSUS_HOST_DISEASE_D7_UP	2.385	.000
ALTEMEIER_RESPONSE_TO_LPS_WITH_MECHANICAL_VENTILATION	2.374	.000
JOHANSSON_GLIOMAGENESIS_BY_PDGFB_UP	2.373	.000
MCBRYAN_PUBERTAL_TGFB1_TARGETS_DN	2.366	.000
STEARMAN_TUMOR_FIELD_EFFECT_UP	2.361	.000
BURTON_ADIPOGENESIS_3	2.357	.000
FLECHNER_BIOPSY_KIDNEY_TRANSPLANT_REJECTED_VS_OK_UP	2.355	.000
MCBRYAN_PUBERTAL_BREAST_4_5WK_UP	2.340	.000
ONDER_CDH1_TARGETS_2_DN	2.328	.000
MCBRYAN_PUBERTAL_BREAST_6_7WK_DN	2.322	.000
ISHIDA_E2F_TARGETS	2.297	.000
KORKOLA_TERATOMA	2.292	.000
LIU_VAV3_PROSTATE_CARCINOGENESIS_UP	2.290	.000
PASINI_SUZ12_TARGETS_DN	2.262	.001
MIKKELSEN_NPC_HCP_WITH_H3K27ME3	2.253	.001
CHANG_CYCLING_GENES	2.253	.001
MOSERLE_IFNA_RESPONSE	2.252	.001
ZHOU_CELL_CYCLE_GENES_IN_IR_RESPONSE_24HR	2.250	.001
BOYLAN_MULTIPLE_MYELOMA_C_D_DN	2.244	.001
PICCALUGA_ANGIOIMMUNOBLASTIC_LYMPHOMA_UP	2.233	.001
WENG_POR_TARGETS_LIVER_UP	2.233	.001
KANG_DOXORUBICIN_RESISTANCE_UP	2.232	.001
ACEVEDO_FGFR1_TARGETS_IN_PROSTATE_CANCER_MODEL_UP	2.231	.001

Supplementary Table 3. Continued

Up-Regulated Chemical and Genetic Perturbation Datasets
Up-Regulated List Truncated at FDR < .005

Database Web Link: (http://www.broadinstitute.org/gsea/msigdb/genesets.jsp?collection=CGP)

Name	NES	FDR *q* Value
MCLACHLAN_DENTAL_CARIES_UP	2.229	.001
LENAOUR_DENDRITIC_CELL_MATURATION_UP	2.226	.001
BROWN_MYELOID_CELL_DEVELOPMENT_UP	2.222	.001
YAGI_AML_FAB_MARKERS	2.216	.001
NAKAYAMA_SOFT_TISSUE_TUMORS_PCA1_UP	2.214	.001
JECHLINGER_EPITHELIAL_TO_MESENCHYMAL_TRANSITION_UP	2.212	.001
TONKS_TARGETS_OF_RUNX1_RUNX1T1_FUSION_ERYTHROCYTE_UP	2.209	.001
YAMASHITA_METHYLATED_IN_PROSTATE_CANCER	2.195	.001
STEARMAN_LUNG_CANCER_EARLY_VS_LATE_DN	2.193	.001
GAL_LEUKEMIC_STEM_CELL_DN	2.193	.001
ODONNELL_TARGETS_OF_MYC_AND_TFRC_DN	2.188	.001
TAKEDA_TARGETS_OF_NUP98_HOXA9_FUSION_10D_UP	2.186	.001
CHIANG_LIVER_CANCER_SUBCLASS_PROLIFERATION_UP	2.163	.001
WALLACE_PROSTATE_CANCER_RACE_UP	2.163	.001
WHITFIELD_CELL_CYCLE_LITERATURE	2.162	.001
MORI_IMMATURE_B_LYMPHOCYTE_UP	2.159	.001
SMID_BREAST_CANCER_LUMINAL_B_DN	2.159	.001
CROONQUIST_NRAS_SIGNALING_DN	2.155	.001
TAKEDA_TARGETS_OF_NUP98_HOXA9_FUSION_8D_DN	2.154	.001
CROONQUIST_IL6_DEPRIVATION_DN	2.151	.001
DELYS_THYROID_CANCER_UP	2.149	.001
MURATA_VIRULENCE_OF_H_PILORI	2.148	.001
LI_INDUCED_T_TO_NATURAL_KILLER_UP	2.144	.001
SERVITJA_ISLET_HNF1A_TARGETS_UP	2.131	.001
HAN_JNK_SINGALING_DN	2.129	.001
WIEDERSCHAIN_TARGETS_OF_BMI1_AND_PCGF2	2.122	.001
BERENJENO_ROCK_SIGNALING_NOT_VIA_RHOA_DN	2.119	.001
GOLDRATH_ANTIGEN_RESPONSE	2.119	.001
ZHOU_CELL_CYCLE_GENES_IN_IR_RESPONSE_6HR	2.115	.001
YU_MYC_TARGETS_UP	2.114	.001
SCHUETZ_BREAST_CANCER_DUCTAL_INVASIVE_UP	2.113	.001
RODWELL_AGING_KIDNEY_NO_BLOOD_UP	2.107	.001
LIAN_LIPA_TARGETS_3M	2.097	.002
TAKEDA_TARGETS_OF_NUP98_HOXA9_FUSION_16D_UP	2.097	.002
SWEET_KRAS_TARGETS_UP	2.096	.002
TSAI_RESPONSE_TO_RADIATION_THERAPY	2.094	.002
MIKKELSEN_MCV6_HCP_WITH_H3K27ME3	2.094	.002
MARTORIATI_MDM4_TARGETS_NEUROEPITHELIUM_DN	2.093	.002
RHODES_UNDIFFERENTIATED_CANCER	2.092	.002
CHIARADONNA_NEOPLASTIC_TRANSFORMATION_KRAS_CDC25_DN	2.090	.002
HAN_JNK_SINGALING_UP	2.089	.002
AMIT_SERUM_RESPONSE_40_MCF10A	2.088	.002
WORSCHECH_TUMOR_EVASION_AND_TOLEROGENICITY_UP	2.087	.002
LIAN_LIPA_TARGETS_6M	2.086	.002
AKL_HTLV1_INFECTION_UP	2.081	.002
OKAMOTO_LIVER_CANCER_MULTICENTRIC_OCCURRENCE_UP	2.081	.002

Supplementary Table 3. Continued

Up-Regulated Chemical and Genetic Perturbation Datasets
Up-Regulated List Truncated at FDR < .005

Database Web Link: (http://www.broadinstitute.org/gsea/msigdb/genesets.jsp?collection=CGP)

Name	NES	FDR *q* Value
LEE_EARLY_T_LYMPHOCYTE_UP	2.080	.002
LABBE_TARGETS_OF_TGFB1_AND_WNT3A_DN	2.080	.002
KATSANOU_ELAVL1_TARGETS_UP	2.079	.002
VANHARANTA_UTERINE_FIBROID_UP	2.074	.002
CHICAS_RB1_TARGETS_GROWING	2.073	.002
RODWELL_AGING_KIDNEY_UP	2.072	.002
VECCHI_GASTRIC_CANCER_ADVANCED_VS_EARLY_UP	2.067	.002
ABRAHAM_ALPC_VS_MULTIPLE_MYELOMA_UP	2.067	.002
LIM_MAMMARY_LUMINAL_MATURE_DN	2.066	.002
KENNY_CTNNB1_ßTARGETS_UP	2.050	.002
BASAKI_YBX1_TARGETS_UP	2.046	.002
LIANG_SILENCED_BY_METHYLATION_UP	2.045	.002
CAVARD_LIVER_CANCER_MALIGNANT_VS_BENIGN	2.038	.003
KEEN_RESPONSE_TO_ROSIGLITAZONE_DN	2.036	.003
DAUER_STAT3_TARGETS_DN	2.035	.003
KAMMINGA_EZH2_TARGETS	2.032	.003
CHANG_IMMORTALIZED_BY_HPV31_DN	2.031	.003
KOBAYASHI_EGFR_SIGNALING_24HR_DN	2.027	.003
JEON_SMAD6_TARGETS_UP	2.022	.003
IGLESIAS_E2F_TARGETS_UP	2.017	.004
DAZARD_UV_RESPONSE_CLUSTER_G24	2.016	.004
SENGUPTA_NASOPHARYNGEAL_CARCINOMA_UP	2.008	.004
ROSS_AML_WITH_CBFB_MYH11_FUSION	2.007	.004
URS_ADIPOCYTE_DIFFERENTIATION_DN	2.006	.004
DAZARD_RESPONSE_TO_UV_SCC_UP	2.006	.004
VERHAAK_AML_WITH_NPM1_MUTATED_UP	2.006	.004
GOBERT_OLIGODENDROCYTE_DIFFERENTIATION_UP	2.004	.004
MEISSNER_BRAIN_HCP_WITH_H3K27ME3	2.001	.004
KAMIKUBO_MYELOID_CEBPA_NETWORK	1.998	.004
VERHAAK_GLIOBLASTOMA_NEURAL	1.997	.004
LIANG_SILENCED_BY_METHYLATION_2	1.992	.004
TURASHVILI_BREAST_LOBULAR_CARCINOMA_VS_LOBULAR_NORMAL_DN	1.989	.005
TAKEDA_TARGETS_OF_NUP98_HOXA9_FUSION_3D_UP	1.980	.005
MCDOWELL_ACUTE_LUNG_INJURY_UP	1.974	.005

Down-Regulated Chemical and Genetic Perturbation Data Sets

Database Web Link: (http://www.broadinstitute.org/gsea/msigdb/genesets.jsp?collection=CGP)

Name	NES	FDR *q* Value
HSIAO_LIVER_SPECIFIC_GENES	−2.829	.000
LEE_LIVER_CANCER_SURVIVAL_UP	−2.743	.000
OHGUCHI_LIVER_HNF4A_TARGETS_DN	−2.645	.000
BILANGES_SERUM_AND_RAPAMYCIN_SENSITIVE_GENES	−2.596	.000
CAIRO_HEPATOBLASTOMA_DN	−2.601	.000
CHIANG_LIVER_CANCER_SUBCLASS_PROLIFERATION_DN	−2.526	.001
BOYAULT_LIVER_CANCER_SUBCLASS_G3_DN	−2.529	.001

Supplementary Table 3. Continued

Down-Regulated Chemical and Genetic Perturbation Data Sets

Database Web Link: (http://www.broadinstitute.org/gsea/msigdb/genesets.jsp?collection=CGP)

Name	NES	FDR *q* Value
CHNG_MULTIPLE_MYELOMA_HYPERPLOID_UP	−2.483	.003
SU_LIVER	−2.408	.011
SHETH_LIVER_CANCER_VS_TXNIP_LOSS_PAM4	−2.351	.025
BOYAULT_LIVER_CANCER_SUBCLASS_G123_DN	−2.327	.028
HOSHIDA_LIVER_CANCER_SUBCLASS_S3	−2.331	.030
SERVITJA_LIVER_HNF1A_TARGETS_DN	−2.310	.030
WOO_LIVER_CANCER_RECURRENCE_DN	−2.314	.030
CAIRO_LIVER_DEVELOPMENT_DN	−2.279	.039
LEE_LIVER_CANCER_ACOX1_DN	−2.241	.051

Note: FDR (false-discovery rate) *q* value: adjusted *P* value; NES, normalized enrichment score.